AD NUMBER

AD-221 626

CLASSIFICATION CHANGES

TO **UNCLASSIFIED**

FROM **CONFIDENTIAL**

AUTHORITY

Tab U60-4-5; Dec 1, 1960, Atchmt 1

19990922123

AD NUMBER

AD-221 626

NEW LIMITATION CHANGE

TO **DISTRIBUTION STATEMENT - A**

Approved for public release;
distribution is unlimited.

LIMITATION CODE: 1

FROM **No Previous DoD Distr Scty Cntrl St'mt Assgn'd**

AUTHORITY

AEDC, via USAF Ltr; May 10, 1971

AD 221 626

DOCUMENT NO. _____
This is copy number 16
of 125, which consists of
47 pages, series A.

(TITLE UNCLASSIFIED)

INVESTIGATION OF HYPERSONIC FLOW OVER BLUNTED PLATES AND CONE

By

J. P. Rhudy, R.S. Hiers, and J. O. Rippey
VKF, ARO, Inc.

May 1960

ARNOLD ENGINEERING DEVELOPMENT CENTER
AIR RESEARCH AND DEVELOPMENT COMMAND
US AF

AEDC-TN-60-93

(Title Unclassified)

INVESTIGATION OF HYPERSONIC FLOW OVER BLUNTED PLATES AND CONE

By

J. P. Rhudy, R. S. Hiers, and J. O. Rippey
VKF, ARO, Inc

May 1960

WADD Project No. 1366, Task No. 14021
ARO Project No. 341020

Contract No. AF 40(600)-800

ABSTRACT

Heat transfer rates and pressure distributions on three basic shapes were investigated at a nominal Mach number of 8 and free-stream Reynolds numbers from 0.43 to 3.4 million per foot. The models were a 0.4-in. nose radius, spherically blunted, 15-deg half-angle cone; two flat plate models with 0.10-in. and 0.50-in. cylindrical blunting; and a modified leading-edge plate with auxiliary planes to produce changing body shape within the elliptic flow region. The tests produced data showing the effect on heat transfer rates of the interaction of the essentially inviscid, rotational flow behind the bow shock with the viscous boundary layer on the body. The results of pressure distribution tests show good agreement with theory. Heat transfer rates over the entire body were accurately predicted through the use of outer-edge boundary-layer conditions obtained from isentropic expansion from normal-shock stagnation conditions.

CONTENTS

ILLUSTRATIONS

NOMENCLATURE

b	Model skin thickness
c	Model material specific heat
c_{p_o}	Specific heat of air at stagnation conditions
h	Enthalpy - based heat transfer coefficient, $\frac{Q_{aero}\ c_{p_o}}{i_o - i_w}$
i_w	Enthalpy of air at model surface temperature
i_o	Enthalpy of air at stagnation conditions
k_δ	Thermal conductivity of air at boundary-layer outer-edge conditions
M	Wind tunnel free-stream Mach number
Nu	Nusselt number, $Nu = \frac{hs}{k_\delta}$ or $\frac{hs_A}{k_\delta}$
p	Model surface pressure
p'	Stagnation pressure behind the normal shock
p_o	Wind tunnel stagnation pressure
Q_{aero}	Aerodynamic heat-flow rate per unit area per unit time
r	Nose radius
Re	Reynolds number, $\frac{\rho_\delta V_\delta s}{\mu_\delta}$ or $\frac{\rho_\delta V_\delta s_A}{\mu_\delta}$
Re_∞	Free-stream Reynolds number
s	Distance along wetted surface of model, measured from zero angle-of-attack stagnation point
s_A	Distance along blunted cone surface measured from the virtual apex of the cone
t	Time
T_o	Wind tunnel stagnation temperature
T_w	Model surface temperature
w	Model material specific weight
α	Angle of attack
θ	Radial angle measured from axis of symmetry
μ_δ	Viscosity of air at boundary-layer outer-edge conditions
ρ_δ	Density of air at boundary-layer outer-edge conditions

INTRODUCTION

At the request of Wright Air Development Division, pressure distribution and heat transfer tests of several basic aerodynamic shapes were conducted for General Applied Science Laboratories, Inc., at a nominal Mach number of 8 and free-stream Reynolds numbers from 0.43×10^6 to 3.4×10^6 per foot. The tests were performed in Tunnel B of the von Karman Gas Dynamics Facility, Arnold Engineering Development Center (VKF-AEDC), December 10-18, 1959. The angle-of-attack range investigated was -15 to +60 deg. Shadowgraphs were taken of each model at each angle of attack at which other data were taken.

The purpose of this test was to provide experimental data at Mach 8 in support of analytical investigations being conducted by General Applied Science Laboratories for Wright Air Development Division. Representative results of the tests are presented herein.

APPARATUS

WIND TUNNEL

Tunnel B is an axisymmetric, continuous-flow, variable-density, hypersonic wind tunnel with a 50-in.-diam test section. Because of changes in boundary-layer thickness due to changing pressure level, the Mach 8 contoured nozzle produces an average test section Mach number which varies from 8.00 at a stagnation pressure of 100 psia to 8.09 at 800 psia. The centerline flow distribution is uniform within about ±1 percent in Mach number, whereas off-center the flow is uniform to about ±0.3 percent. There is a slight axial gradient on the order of 0.01 Mach number per foot.

Details of Tunnel B and associated equipment are shown in Fig. 1. The hydraulically driven angle-of-attack sector pitches the model in a vertical plane from -15 to +15 deg with a straight sting and from -15 to +60 deg with a set of adapters supplied by General Applied Science Laboratories. The remotely controlled, water-cooled, roll mechanism is electrically driven and is capable of rotating the model-sting combination from -185 to +180 deg.

Stagnation pressures up to approximately 800 psia are supplied to Tunnel B by the VKF Compressor Plant. The air is selectively valved through the Compressor Plant, the high-pressure driers, and the propane-fired heater. The heater produces a maximum air temperature of 900°F, sufficient to prevent liquefaction of the air in the test section. From the heater, the air flows through the nozzle, the diffuser, the cooler, and back into the compressor system.

Manuscript released by authors April 1960.

COOLING SHOES

Between data runs in the heat transfer phase, the model was enclosed in cooling shoes into which cold air was introduced to cool the model. These shoes (split in the vertical plane) were retracted to the tunnel walls for taking heat transfer data. The hydraulically actuated cooling-shoe mechanisms were mounted in place of the windows as shown in Fig. 2. The cooling shoes were of sufficient cavity size to allow pitching all models to the test angle of attack prior to opening the shoes (Fig. 3).

MODELS AND SUPPORT

The models were of three shapes: a 0.40-in. radius, spherically blunted, 15-deg half-angle cone (Fig. 4), two cylindrically blunted flat plates of 0.10-in. and 0.50-in. nose radius (Figs. 5 and 6), and a 0.50-in. radius cylindrically blunted, modified leading-edge flat plate (Fig. 7). The models were fabricated of type 304 stainless steel. Three adapters, split on the vertical center plane (Fig. 8), were provided to allow change of the angle-of-attack range of the tests without disassembly of the model setup.

The cone model for pressure testing was supplied with fifty-four static pressure taps arranged on rays along the conical surface. The cone used for heat transfer testing was provided with fifty-four, No. 30 gage, chromel-alumel thermocouples located in the same positions as the respective pressure taps on the pressure cone. The skin thickness of the pressure cone was 0.250 in. thick, whereas the heat transfer cone thickness was 0.050 in.

The flat plate models, including the modified leading-edge model, were of 0.19-in. thick plate construction with the thermocouple-instrumented strip milled to 0.050-in. thickness (Fig. 9). The 0.10-in. nose radius plate was equipped with thirty-eight thermocouples and forty pressure taps. The 0.50-in. nose radius plate contained fifty-one thermocouples and fifty-five pressure taps, and the modified leading-edge plate was provided with thirty-two thermocouples and thirty-two pressure taps.

The thermocouples were installed using the method of Ref. 1. In this method, a hole of 0.040-in. diam is drilled through the model skin at the desired junction location. The outer insulation is stripped from the thermocouple lead, and the two wires, with their secondary insulation intact, are drawn through the drilled hole. A flat-faced, tapered pin of the same material as the model skin is driven into the hole until the resistance of the two wires reads substantially the same as though the two wires had been touched together at the model. The pin is sheared at the inside and outside model surfaces and the pin thickness is measured. The junction must show quick response to a touch of a hot iron, or the assembly is knocked out and a new junction is formed.

The models were supported in the tunnel on a straight uncooled sting. The conversion from -15 to +15-deg angle of attack to other angle-of-attack ranges was accomplished by the GASL-supplied adapters (Fig. 10). Figure 11 shows the model instrumented regions.

INSTRUMENTATION

Pressure Distribution Phase

The model pressures were measured with nine Wiancko pressure transducers, rated at 5 psid and selectively connected to three independently variable reference pressure systems. The three reference systems were constantly monitored by CEC Electromanometers with 1, 5, and 15 psid capacities. An essentially zero pressure system was used on the reference side of the Electromanometers.

The pressure side of each Wiancko transducer was inserted into the outlet of a Giannini 12-position rotary valve. Reference pressure was connected to the first valve inlet position to obtain the instrument zero. Various model pressure taps were connected in the desired order to the required number of the remaining eleven valve inlets. The transducer outputs were measured with Leeds and Northrup self-balancing, millivolt potentiometers equipped with Coleman digital read-out units. The potentiometer readings were punched on paper tapes by a high-speed punch.

Heat Transfer Phase

The reference junction of each thermocouple was maintained at 32°F. Each thermocouple output was recorded in digital form on magnetic tape at a rate of four times per second by means of a Consolidated Electro-dynamics Corporation Millisadic analog-to-digital converter. To monitor the temperatures at selected points on the models, six of the thermocouple outputs were observed prior to the data run on 0.25 sec (full-scale travel) Brown servo-potentiometers.

General

The tunnel stagnation pressure and temperature were measured in the stilling chamber. A 1000-psid transducer, referenced to atmosphere, and a chromel-alumel thermocouple were used for the measurement. A conventional, short-range, divergent-ray, spark shadowgraph system was used to record selected flow patterns about the model.

PROCEDURE

TEST PROCEDURE

The heat transfer cone and the three heat transfer pressure distribution plate models were pitched to the test angle of attack and cooled

until a nearly uniform surface temperature of 500°R was obtained. The cooling air supply was then shut off, and the cooling shoes were withdrawn to the tunnel sidewalls. Approximately 0.4 sec was required to move the cooling shoes sufficiently far from the model so that no flow disturbance impinged on the model. In the case of the heat transfer cone, 20 sec of temperature-time data were recorded, the cooling shoes were replaced over the model, and the cycle repeated.

Pressure measurement was begun on the flat plate models after the instruments stabilized, and about five minutes of model exposure to the airstream were required to complete them. During this time the temperature measurement continued.

The cone pressure model was tested with the cooling shoes removed from the tunnel and with the flow observation windows in place. Pressure measurement required about five minutes at each test condition. Shadowgraph photographs were taken during these runs.

The test conditions for each model were:

1. 0.40-in. radius, spherically blunted, 15-deg half-angle cone models

α	Increment of α	Re_∞ /ft x 10^{-6}
0 - 20	2.5	0.43, 1.0, 2.6
20 - 30	5	0.43, 1.0, 2.6
30 - 50	10	2.6

2. 0.10-in. nose radius model

α	Increment of α	Re_∞ / ft x 10^{-6}
0 - 20	2.5	0.43, 1.0, 2.0
20 - 30	5	0.43, 1.0, 2.0
30 - 40	10	0.43
0 - 15	5	3.4

3. 0.50-in. nose radius model

α	Increment of α	Re_∞ / ft x 10^{-6}
0 - 20	2.5	0.43, 1.0, 2.0
20 - 30	5	0.43, 1.0, 2.0

4. 0.50-in. nose radius, modified leading-edge model

α	Increment of α	Re_∞ / ft x 10^{-6}
-15 - +6	3	2.0
10 - 30	5	2.0

DATA REDUCTION PROCEDURE

The ratio p/p' was calculated using the measured pressure p and a value of p' obtained from the expression

$$p' = \left(\frac{6M^2}{M^2 + 5}\right)^{7/2} \left(\frac{6}{7M^2 - 1}\right)^{5/2} (p_o)$$

The values of M used in the data reduction were:

Re_∞ / ft	M
0.43×10^6	8.00
1.00×10^6	8.03
2.00×10^6	8.08
2.60×10^6	8.08
3.40×10^6	8.09

The value of p_o used was that measured at the same time the model static pressure was measured.

The heat transfer data were reduced using the equation

$$Q_{aero} = wbc \frac{dT_w}{dt}$$

All losses were ignored. Two values of T_w and $\frac{dT_w}{dt}$ were obtained by fitting parabolas by the method of least squares to the nine data points centered at times one and five seconds after the cooling shoes were against the tunnel wall. A heat transfer coefficient based on enthalpy was calculated using the following formula:

$$h = \frac{Q_{aero} c_{p_o}}{i_o - i_w}$$

The thermodynamic properties of air used are those of Table A-3 of Ref. 2.

The Nusselt number was calculated using the relation

$$Nu = \frac{hs}{k_\delta}$$

for the flat-plate models and

$$Nu = \frac{hs_A}{k_\delta}$$

for the blunted cone model.

The Reynolds numbers calculated were

$$Re = \frac{\rho_\delta V_\delta s}{\mu_\delta}$$

for the flat-plate models and

$$Re = \frac{\rho_\delta V_\delta s_A}{\mu_\delta}$$

for the blunted cone model.

The air properties used to calculate these values were taken from Table A-4 of Ref. 3. The functions of M were obtained from Ref. 8.

RELIABILITY OF DATA

The reliability of the pressure measurement varied with region of the model and with tunnel stagnation pressure level. This reliability is:

Re_∞/ft	Region of Model	Percent Error in p/p'
0.43×10^6	Stagnation	± 6.0 max
2.60×10^6	Stagnation	± 3.0 max
0.43×10^6	From Shoulder Aft	± 5.0 max
3.40×10^6	From Shoulder Aft	± 1.5 max

The measurement of heat transfer in the stagnation region of the models was unsatisfactory because of high conduction losses associated with the small nose radii. In the range of $Nu/\sqrt{Re}$ from 0.5 to 0.1 found to exist over the major portion of the models, the repeatability of $Nu/\sqrt{Re}$ was from 0.10 to 0.03, respectively, for the data presented.

RESULTS AND DISCUSSION

BLUNTED CONE

In Fig. 12, the axial pressure distribution on the blunted cone is shown for several angles of attack. At small angles of attack the surface pressure is predicted most accurately by the equivalent cone method (Ref. 4). For large angles of attack, the modified Newtonian value is more accurate. The peripheral pressure distribution is given for several angles of attack in Fig. 13, with the experimental fit method of Zakkay (Ref. 5) applied to the data. The computed variation fits the experimental variation fairly well.

The variation with s/r of $Nu/\sqrt{Re}$ is shown in Fig. 14 for zero angle of attack. Comparison is made with the theoretical variation of this parameter, obtained using Lees' method (Ref. 6), with the boundary-layer outer-edge conditions behind the shoulder calculated using normal-shock stagnation conditions with the measured surface pressures and the stagnation point value of Fay and Riddell (Ref. 7). The values from experiment and those given by theory agree closely and indicate that the normal-shock-affected streamlines cover the viscous layer for all Reynolds numbers at which tests were conducted.

FLAT PLATES

The pressure distribution on both flat plates (Fig. 15) tends toward the wedge value given in Ref. 8. In the stagnation region of the 0.50-in. nose radius plate, the numerical solution of Van Dyke (Ref. 9) calculated for M tending to infinity agrees closely with the experimental pressure data. Beyond the limit of the numerical solution, a combination of modified-Newtonian and Prandtl-Meyer expansion is shown. This method (Ref. 10) gives results which are lower than experiment.

The pressure distribution in the leading-edge region of the modified leading-edge model (Fig. 16) shows a marked change with location of the sonic points. For the angles of attack for which both sonic points are on the cylinder (-12 deg, -6 deg), the pressure distribution agrees with that given by theory for a circular cylinder. For angles of attack of 0 deg and above, the experimental pressure distribution shows a slower change in pressure with distance along the surface. This is in agreement with the results presented in Ref. 11 for a similar configuration tested at Mach 6 and is the result of the movement of one sonic point onto the plane tangent to the cylinder near the zero angle-of-attack body sonic point.

Values of the heat transfer parameter, $Nu/\sqrt{Re}$, are presented in Fig. 17 for the cylindrically blunted flat plate models. The theoretical distributions were calculated using Lees' theory (Ref. 6). The boundary-layer outer-edge conditions used were free-stream conditions and local conditions based on measured static pressure and stagnation pressure behind a normal shock. The results show that the normal-shock-affected streamlines cover the boundary layer and that the assumption that the boundary-layer outer-edge flow expands isentropically from stagnation point conditions gives good accuracy for heat transfer rate prediction. Stagnation point heating rates are not given for the models because conduction losses made the data in this region inconclusive.

CONCLUSIONS

Within the range of free-stream conditions of this test, the following conclusions may be drawn:

1. The "experimental fit" method of Zakkay accurately predicts the pressure distribution on blunted cones at angle of attack.

2. The "modified Newtonian" pressure distribution for cones at angle of attack increases in accuracy with increasing angle of attack.
3. The "equivalent cone" pressure distribution increases in accuracy as the angle of attack is reduced toward zero.
4. The pressure distribution on a cylindrical nose is given accurately by the M = ∞ solution of Van Dyke. This is in agreement with the theory that stagnation region pressure distributions on spheres and cylinders change very little above M of about 2 to 3.
5. The shape of the body between the sonic points has a marked effect on the pressure distribution in this region.
6. For M = 8 and Reynolds number based on free-stream conditions and body nose radius greater than about 4000, the use of normal-shock stagnation pressure with local static pressure to calculate boundary-layer outer-edge conditions yields accurate heat transfer rates for ratios of length to nose radius up to 100.

REFERENCES

1. Zakkay, Victor. "Pressure and Laminar Heat Transfer Results in Three-Dimensional Hypersonic Flow." WADC-TN-58-182, September 1958.
2. Cambel, Ali Bulent. Gas Dynamics. McGraw-Hill Book Company, New York, 1958.
3. Eckert, E. R. G. and Drake, R. M., Jr. Heat and Mass Transfer. McGraw-Hill Book Company, New York, 1959.
4. Zakkay, Victor. "An Investigation of the Pressure Distribution on Conical Bodies in Hypersonic Flow." Journal of the Aero/Space Sciences, Vol. 26, No. 7, July 1959, p. 457.
5. Zakkay, Victor. "Laminar Heat-Transfer and Pressure Measurements Over Blunt-Nosed Cones at Large Angle of Attack." Journal of the Aero/Space Sciences, Vol. 25, No. 12, December 1958, pp. 794 - 795.
6. Lees, Lester. "Laminar Heat Transfer Over Blunt-Nosed Bodies at Hypersonic Flight Speeds." Jet Propulsion, Vol. 26, No. 4, April 1956, pp. 259 - 269, 274.
7. Fay, J. A. and Riddell, F. R. "Theory of Stagnation Point Heat Transfer in Dissociated Air." Journal of the Aeronautical Sciences, Vol. 25, No. 2, February 1958, pp. 73 - 85, 121.
8. Ames Research Staff. "Equations, Tables, and Charts for Compressible Flow." NACA Report 1135, 1953.

9. Van Dyke, Milton D. "The Supersonic Blunt-Body Problem - Review and Extension." Journal of the Aero/Space Sciences, Vol. 25, No. 8, August 1958, pp. 485 - 496.

10. Wagner, Richard D., Jr. "Some Aspects of the Modified Newtonian and Prandtl-Meyer-Expansion Method for Axisymmetric Blunt Bodies at Zero Angle of Attack." Journal of the Aero/Space Sciences, Vol. 25, No. 12, December 1959, pp. 851 - 852.

11. Ferri, Antonio and Zakkay, Victor. "Pressure Distributions for a Two-Dimensional Blunt-Nosed Body at Different Angles of Attack." Journal of the Aero/Space Sciences, Vol. 26, No. 6, June 1959, pp. 395 - 396.

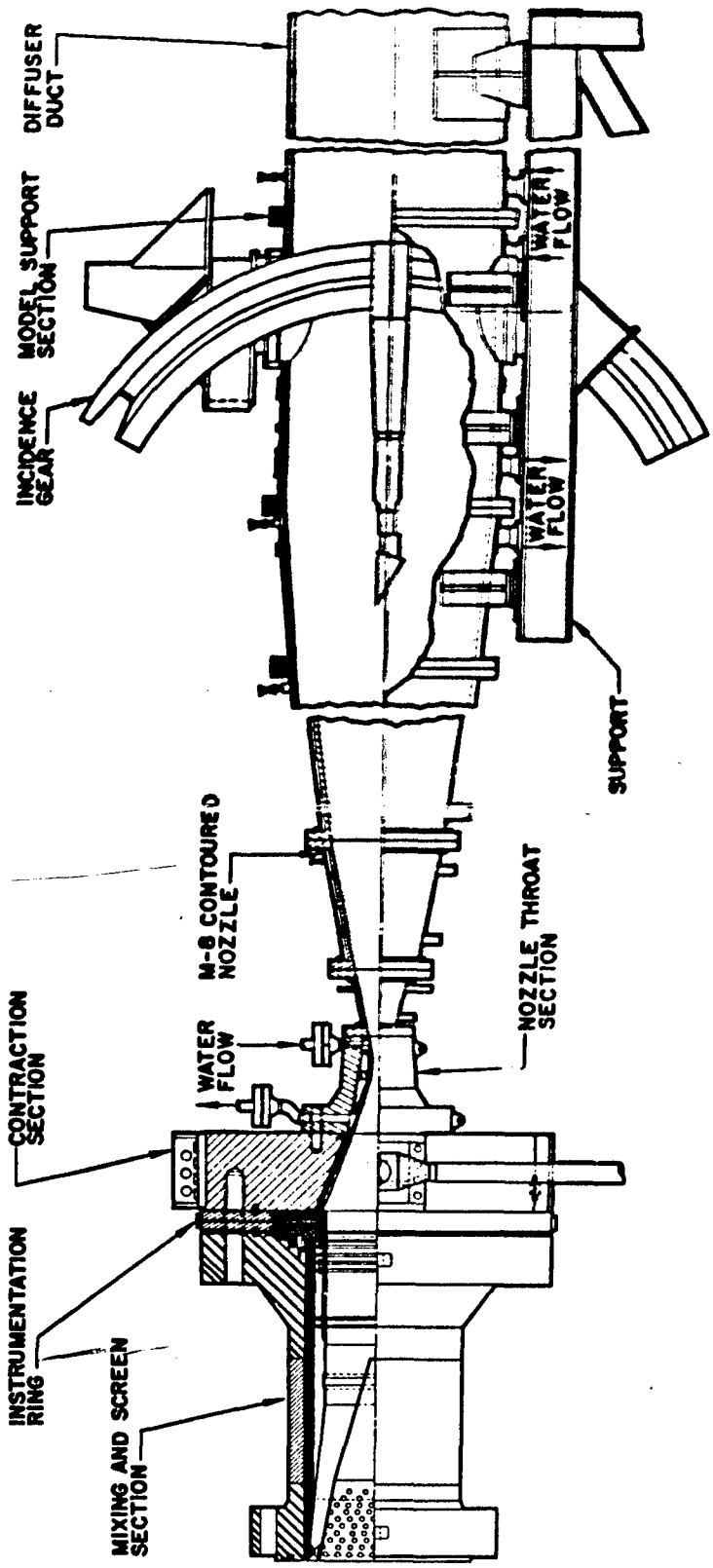

Fig. 1 Tunnel B and Associated Equipment

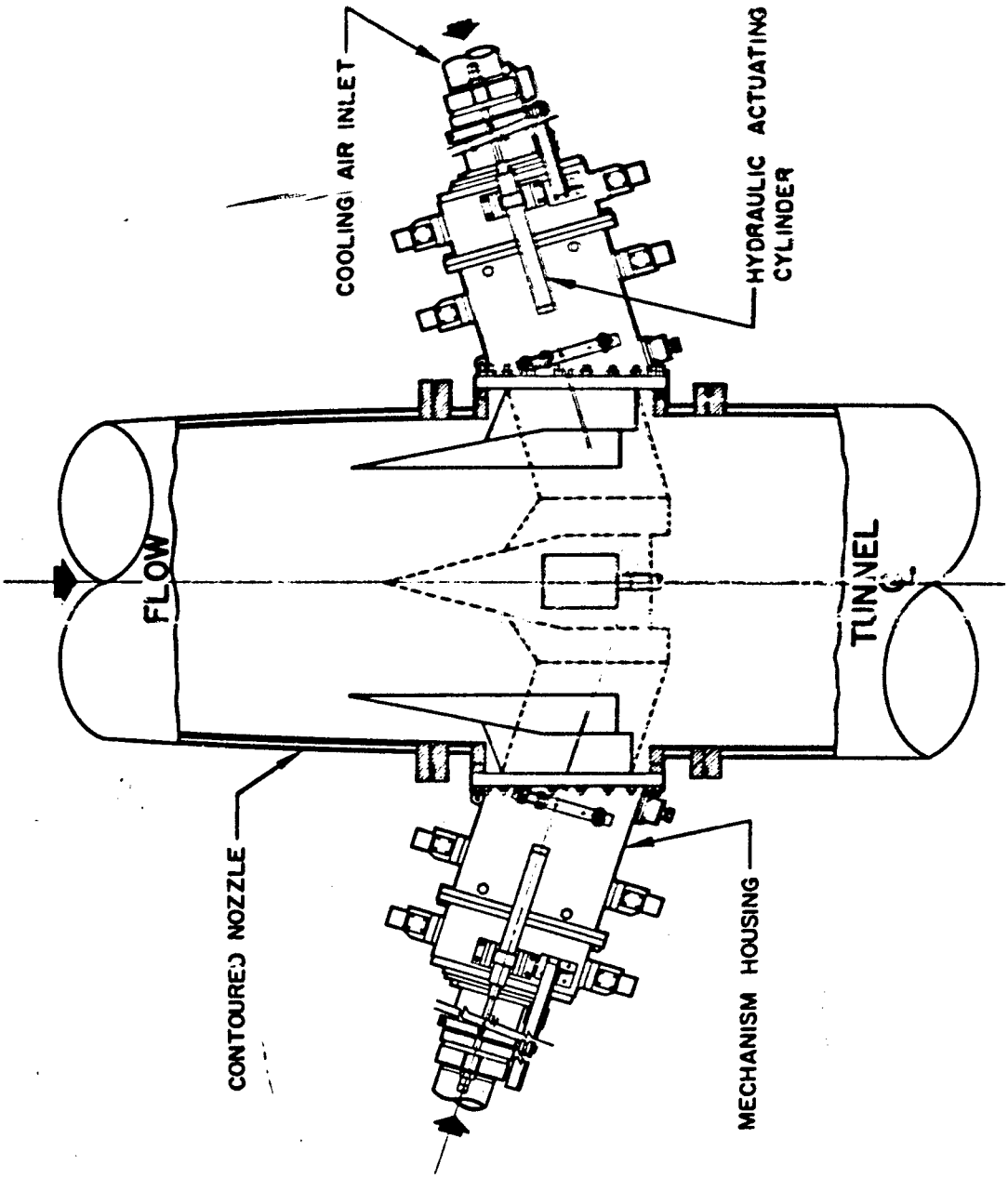

Fig. 2 Cooling Shoe Mechanism with Flat Plate Model in Test Position

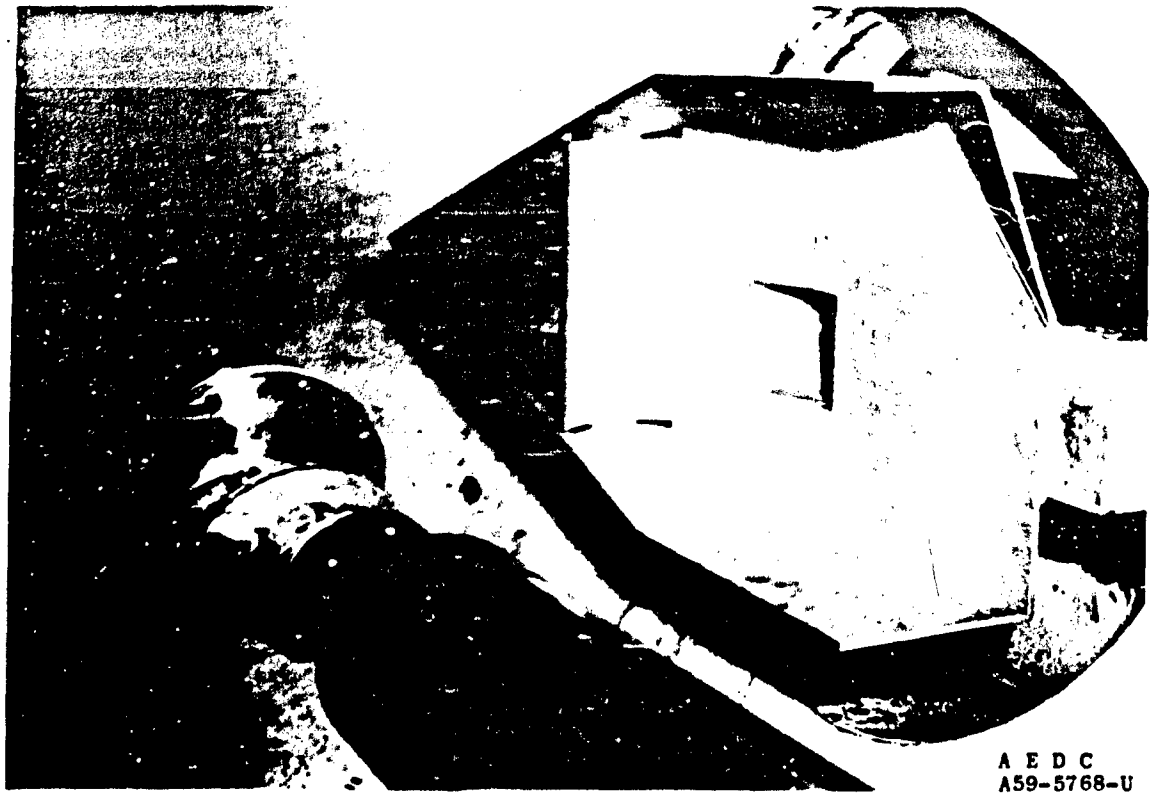

a. Rear View, Shoes Open

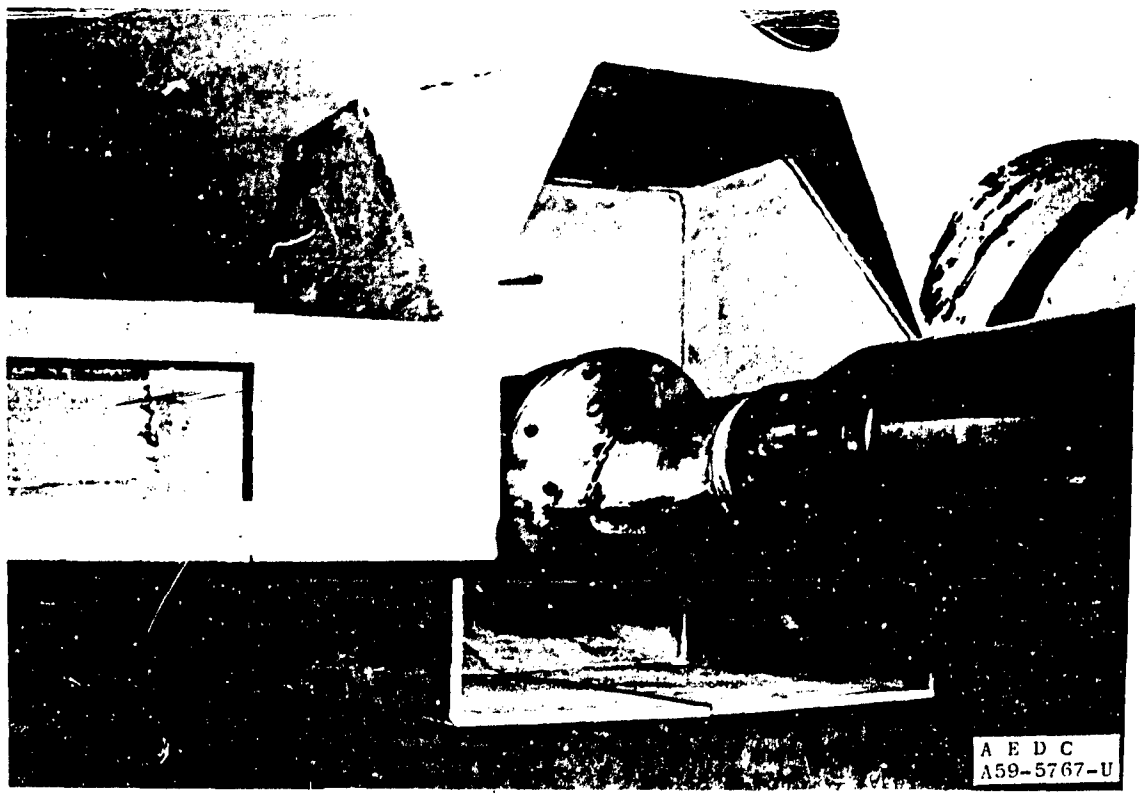

b. Rear View, Shoes Closed

Fig. 3 Cooling Shoes

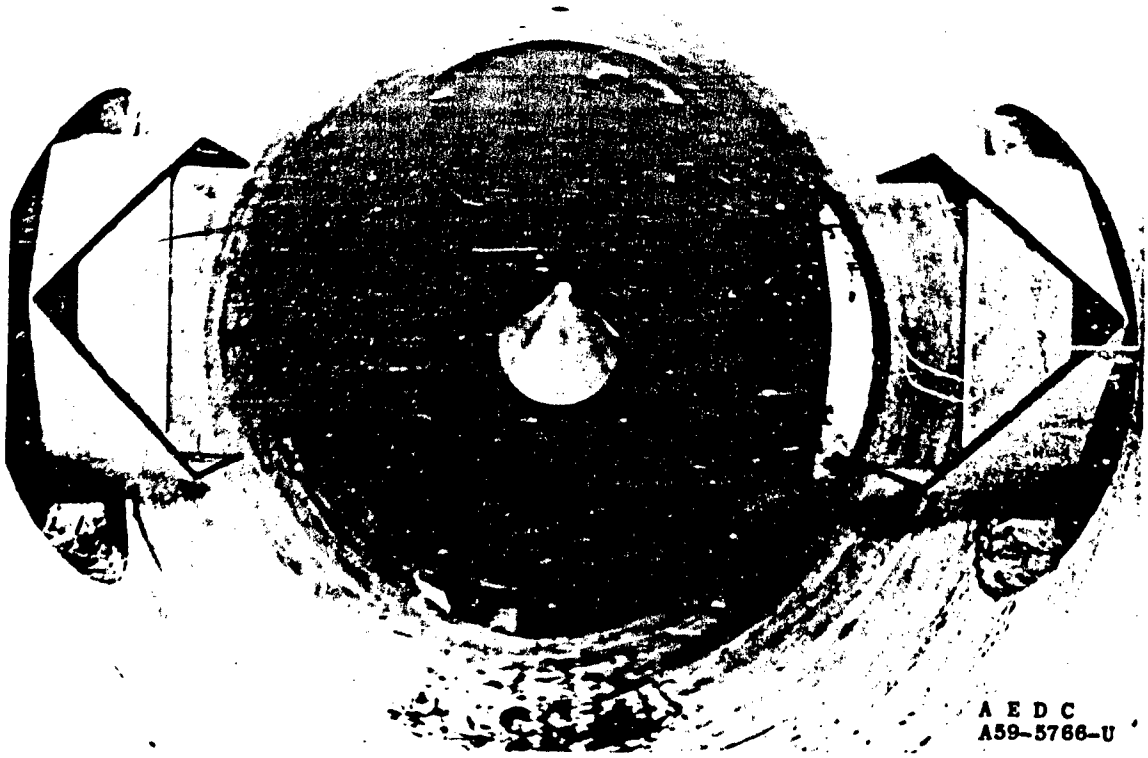

c. Front View, Shoes Open

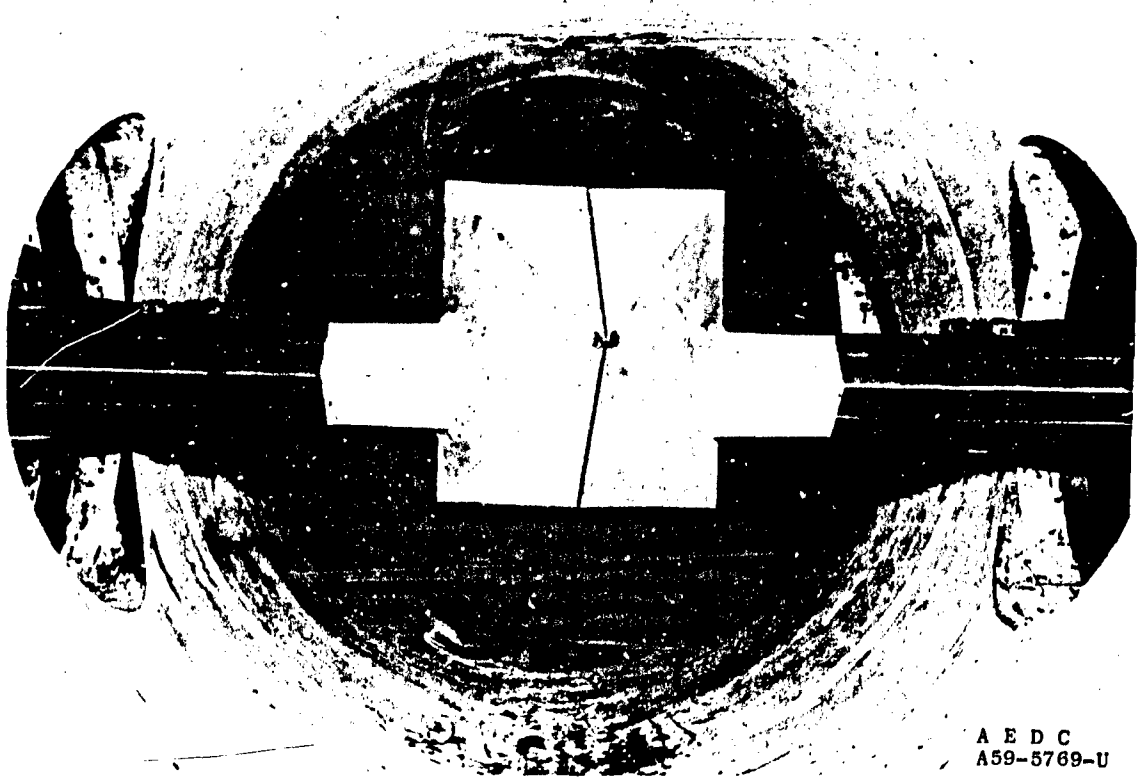

d. Front View, Shoes Closed
Fig. 3 Concluded

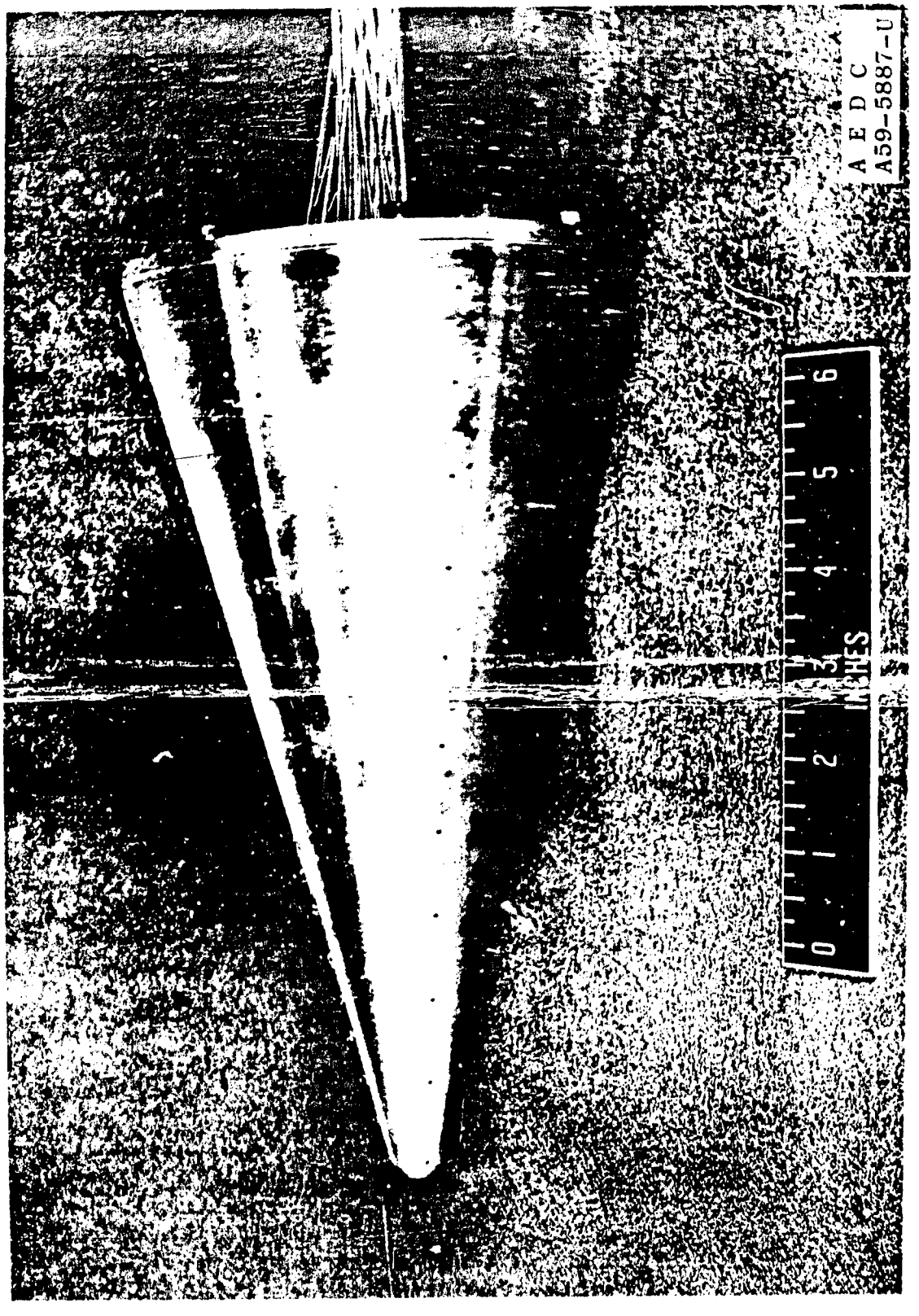

Fig. 4 0.40-in. Spherically Blunted, 15-deg Half-Angle Cone

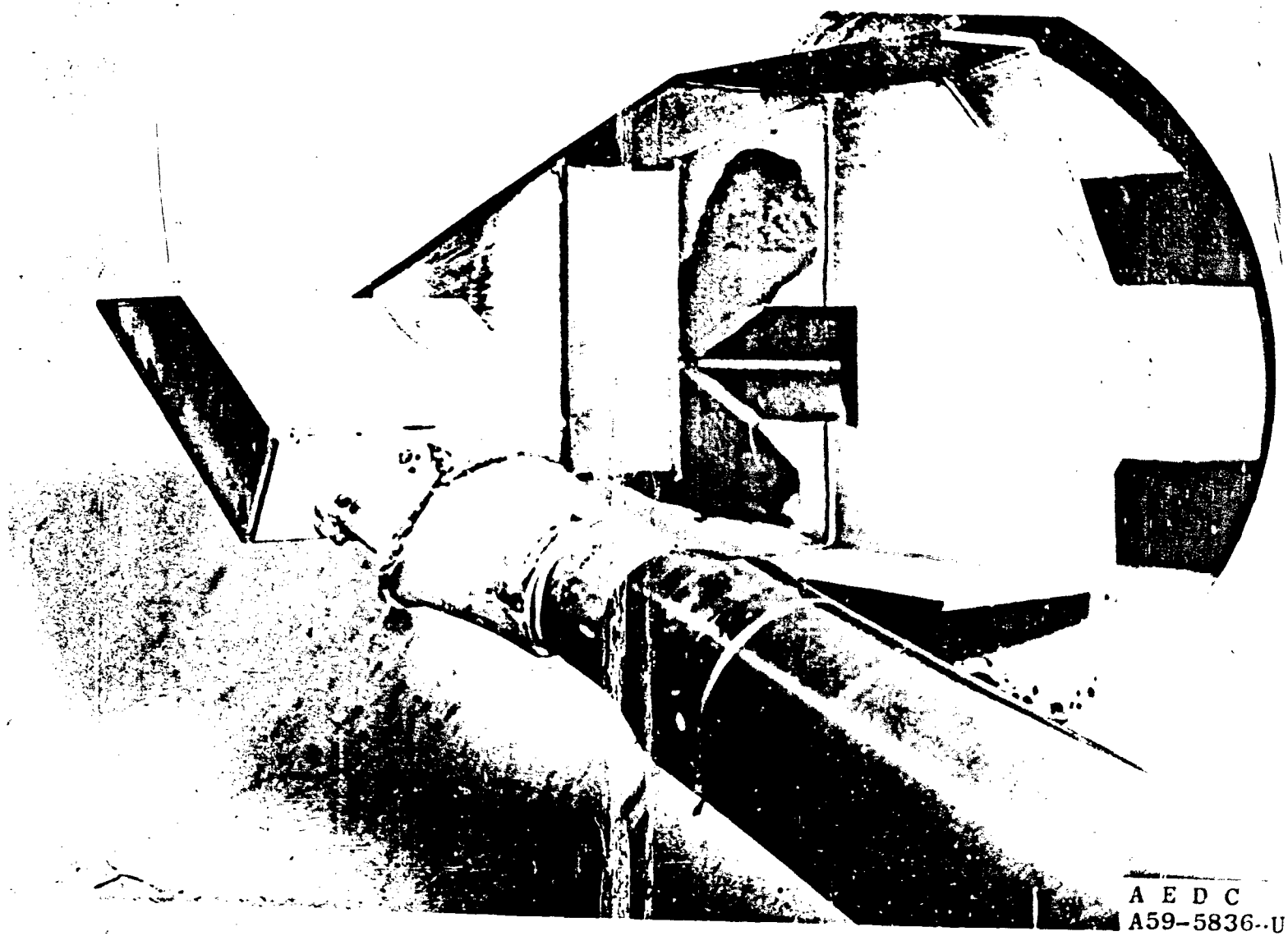

Fig. 5 0.10-in. Nose Radius Flat Plate Model Installed in Tunnel B

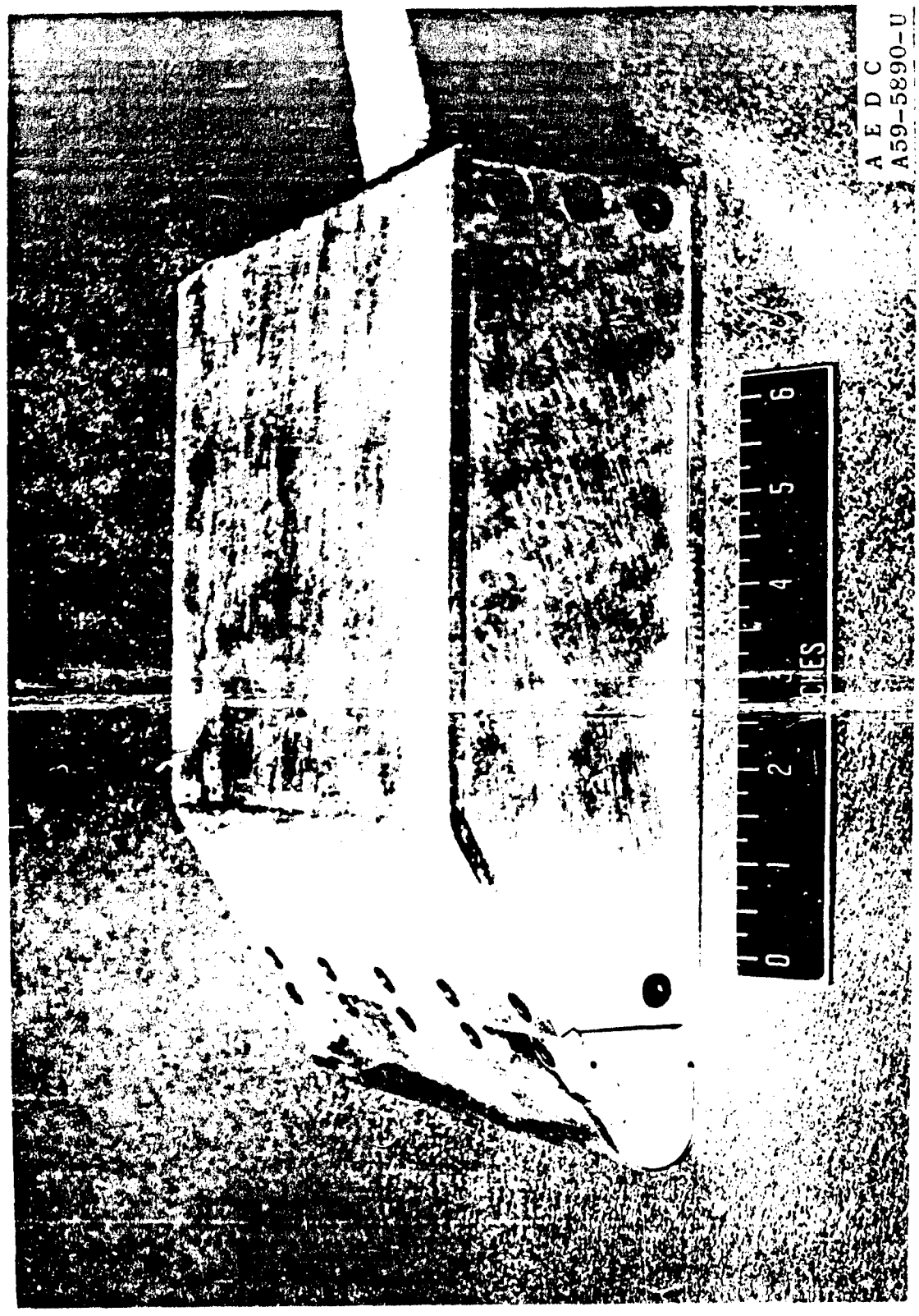

Fig. 6 0.5[illegible]-in. Nose Radius Flat Plate Model

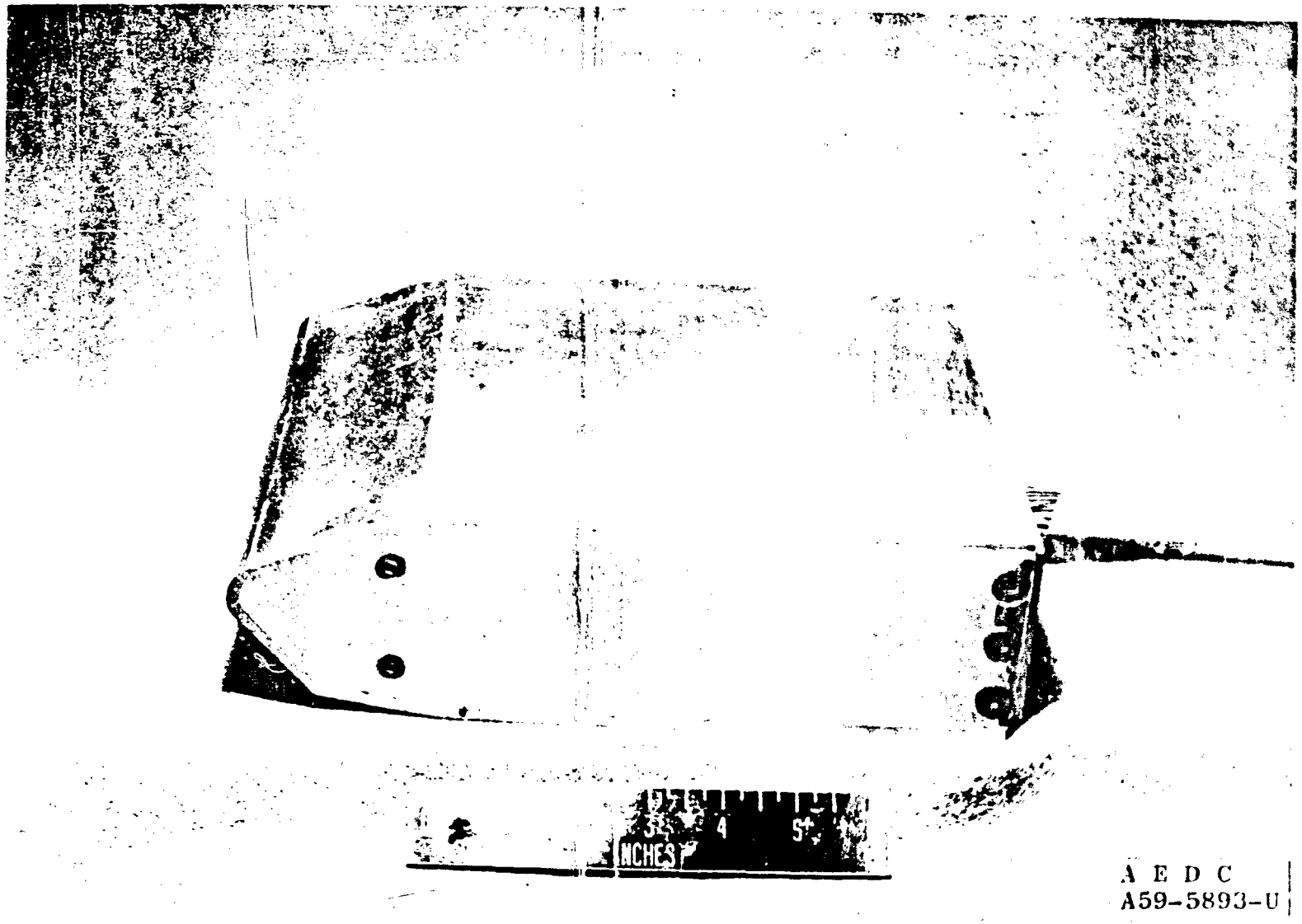

Fig. 7 0.50-in. Modified Leading-Edge Flat Plate Model

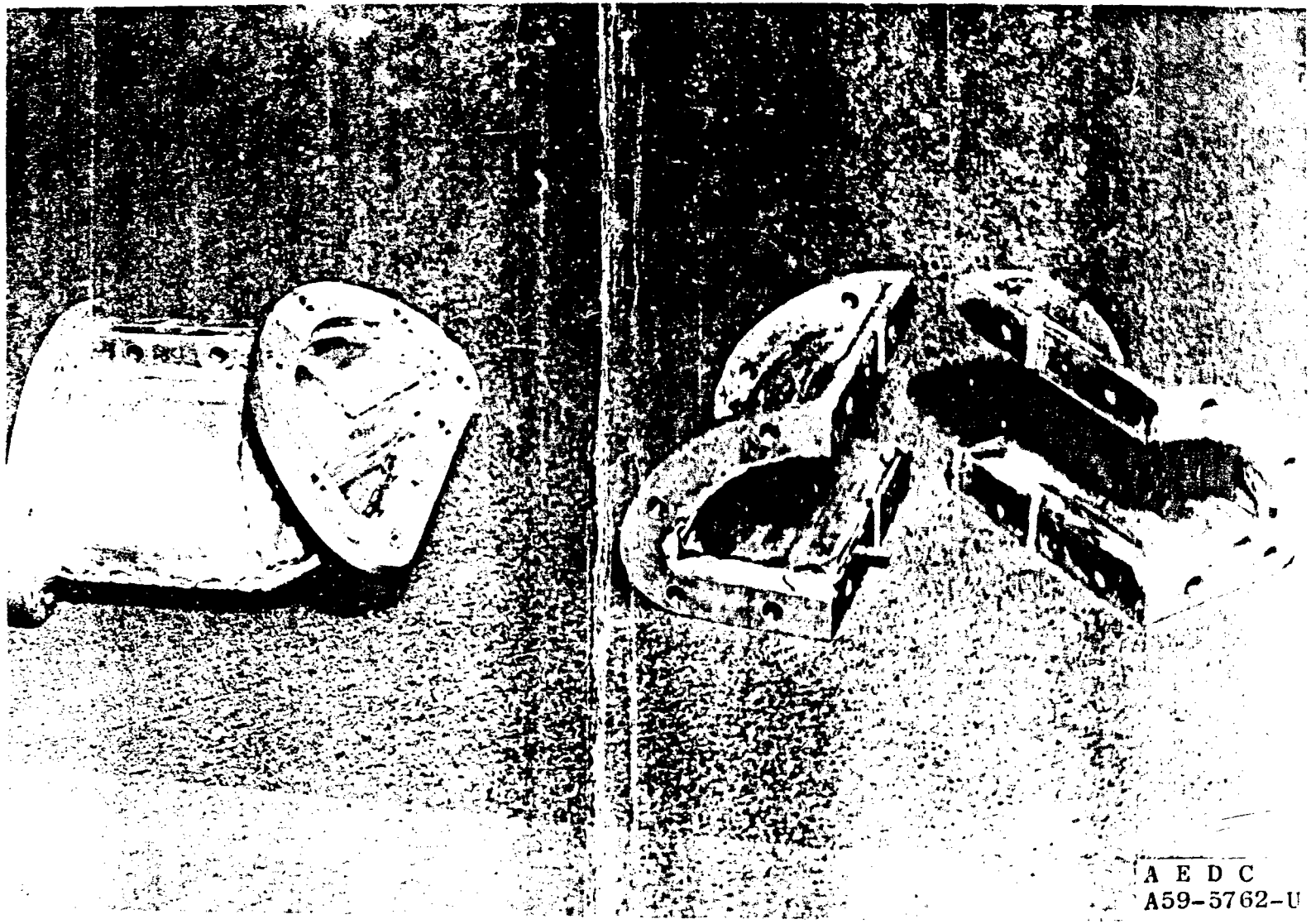

Fig. 8 Angle-of-Attack Adapters

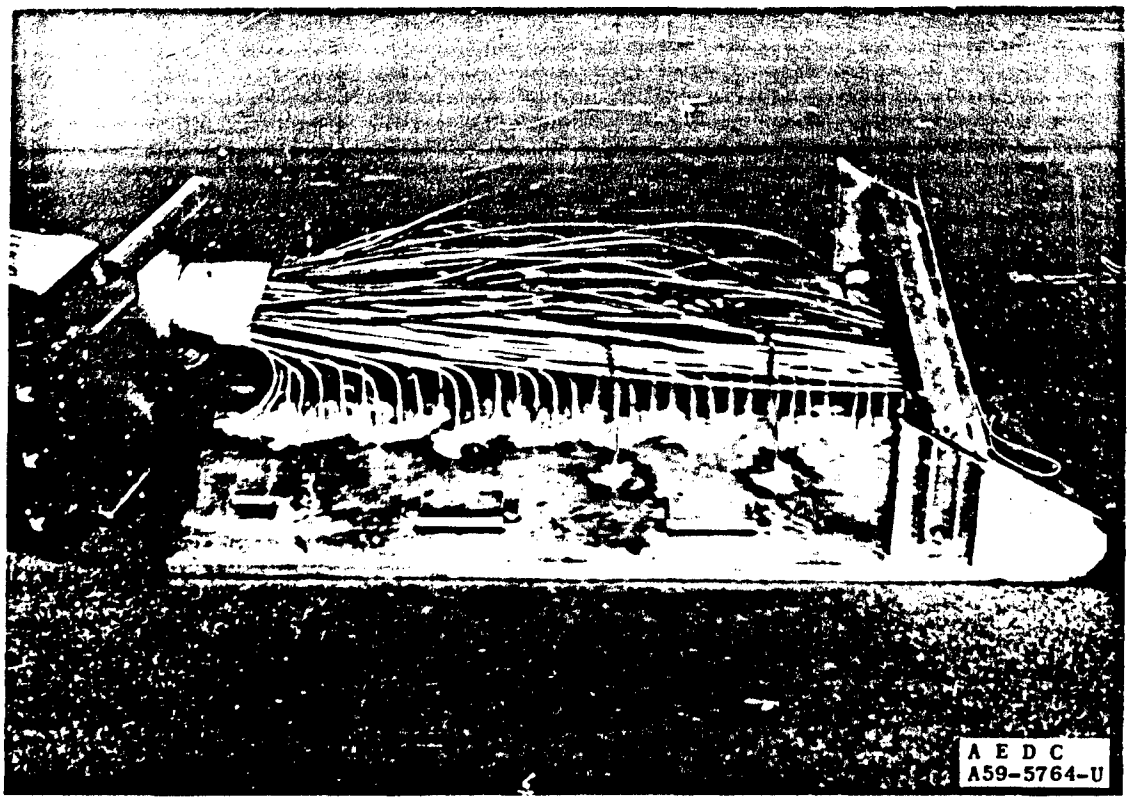

a. Pressure Side

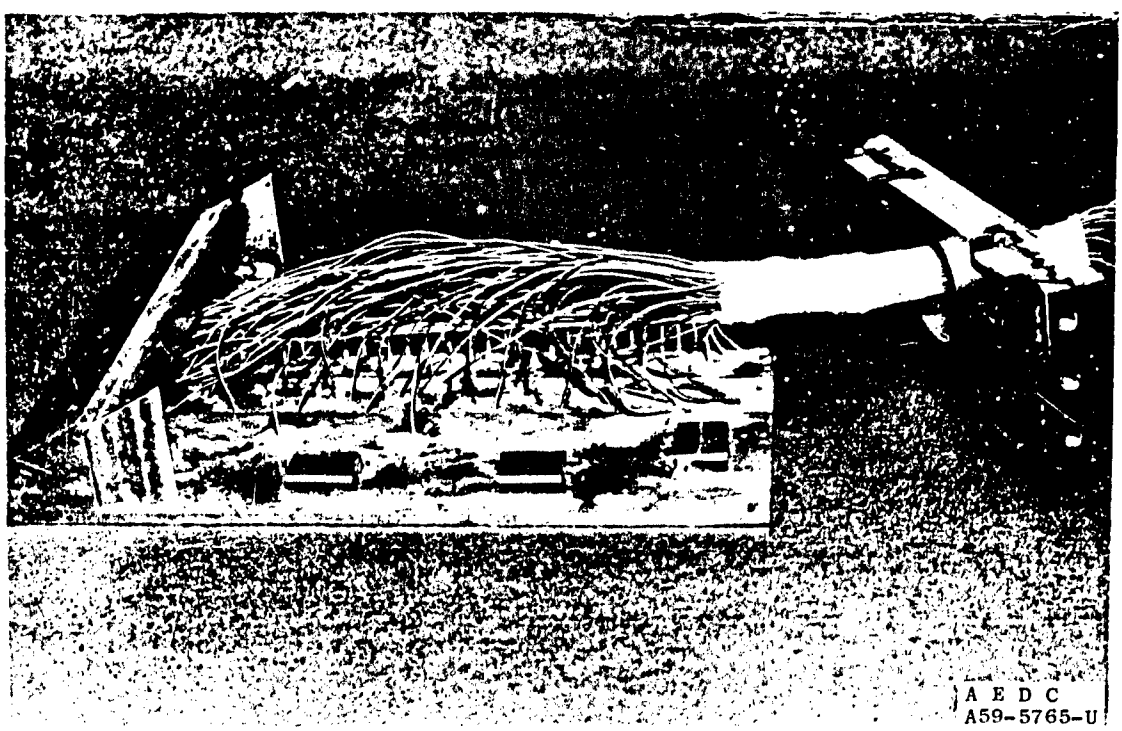

b. Thermocouple Side

Fig. 9 0.50-in. Nose Radius Flat Plate Model Instrumentation

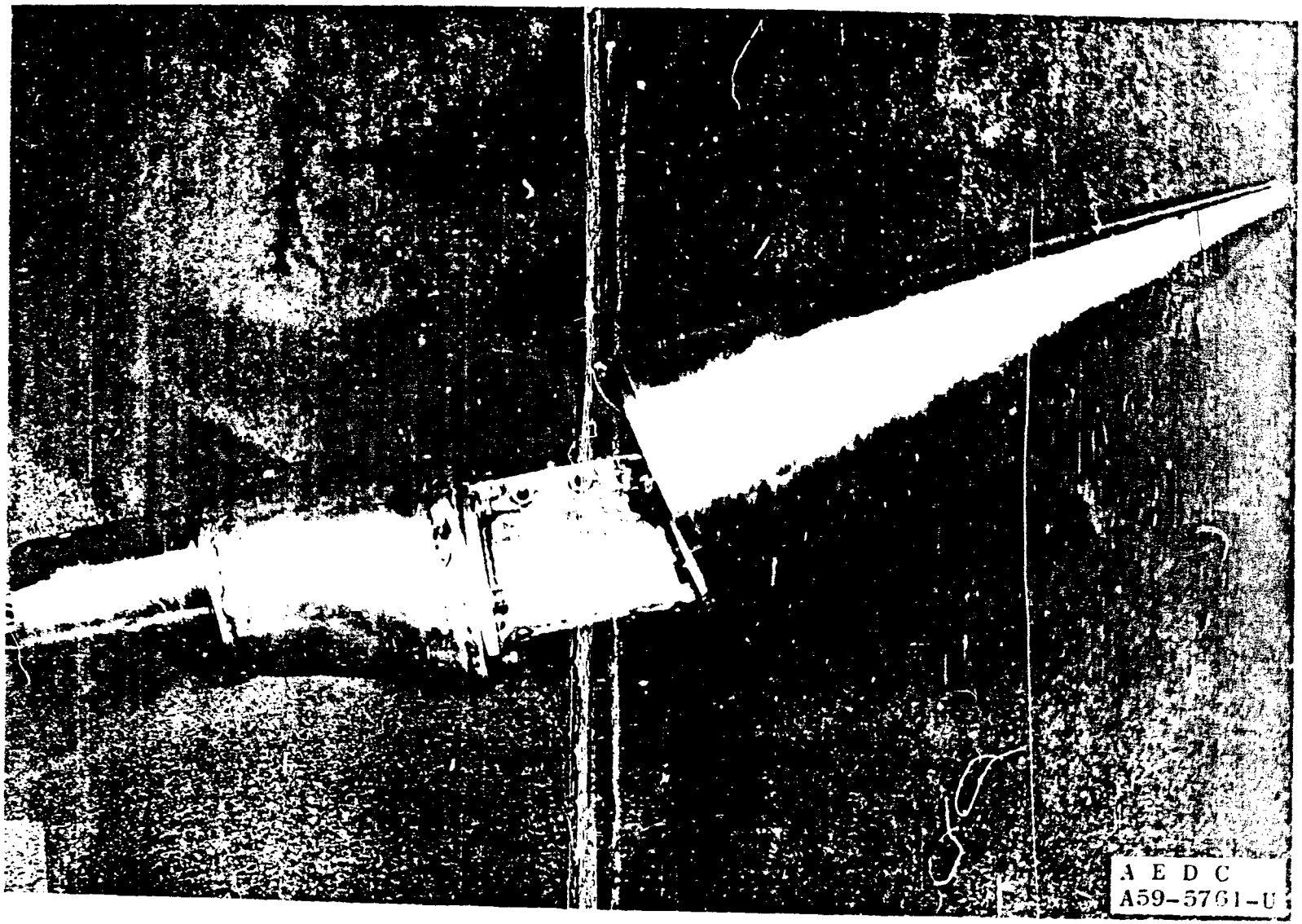

Fig. 10 Cone Model on 0 to 30-deg Angle-of-Attack Adapter

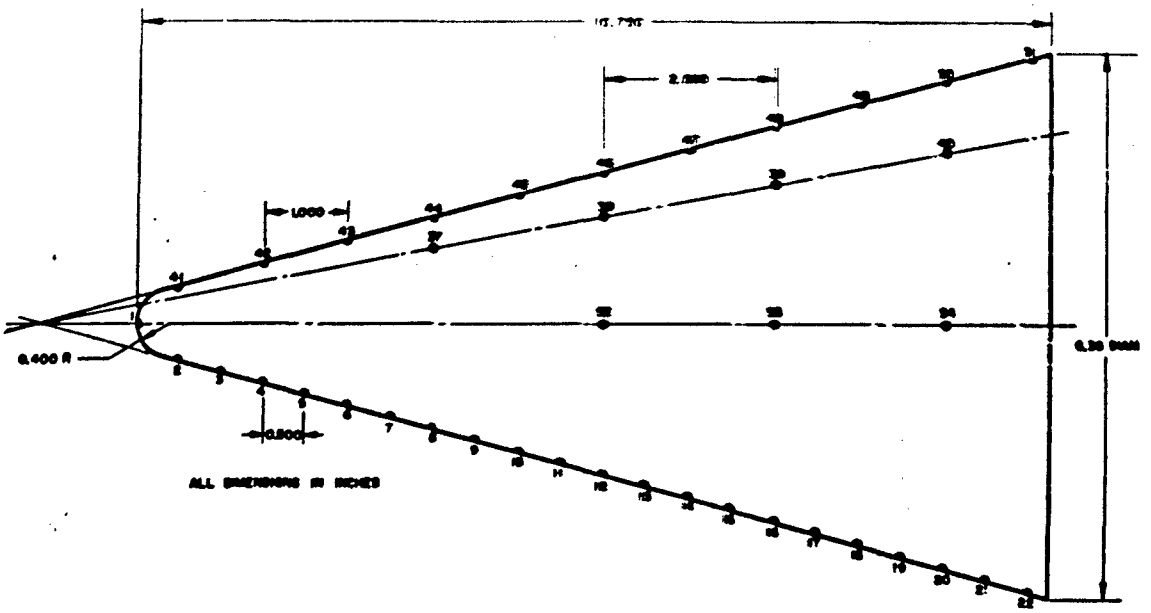

a. Cone Model, Side View

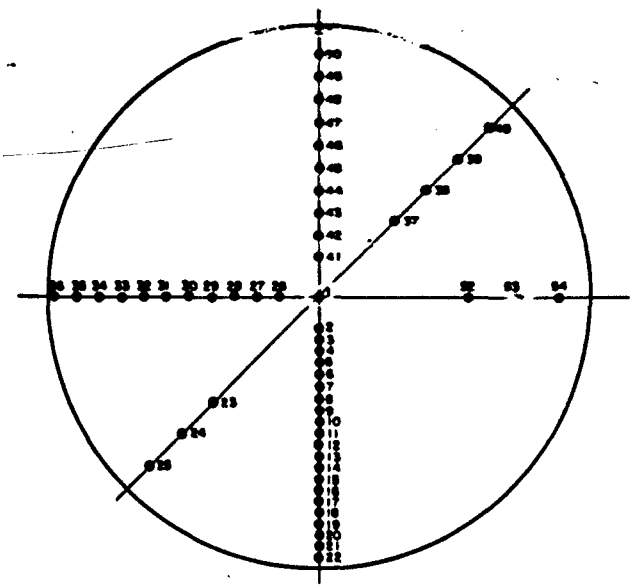

b. Cone Model, Front View

Fig. 11 Model Instrumentation Regions

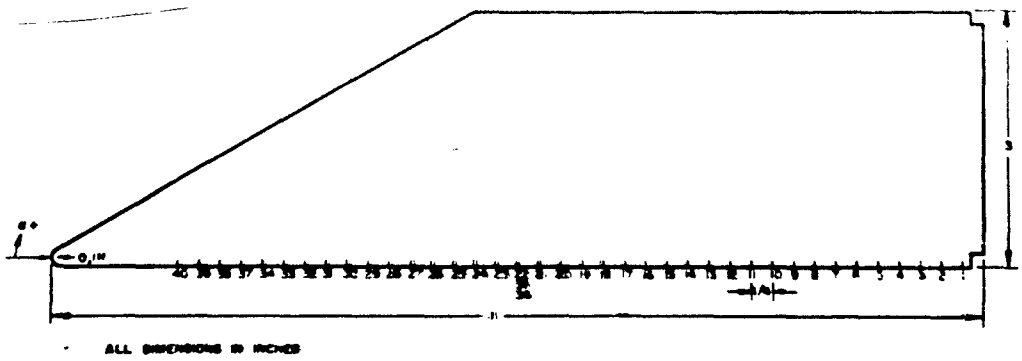

c. 0.10-in. Nose Radius Flat Plate Model

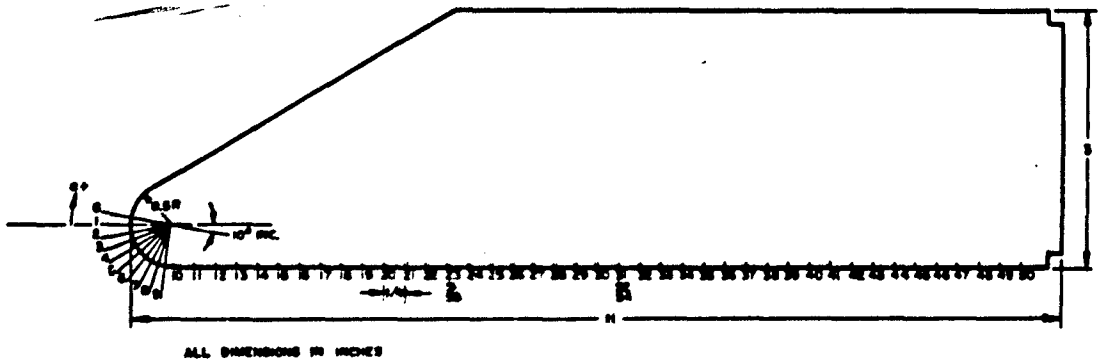

d. 0.50-in. Nose Radius Flat Plate Model

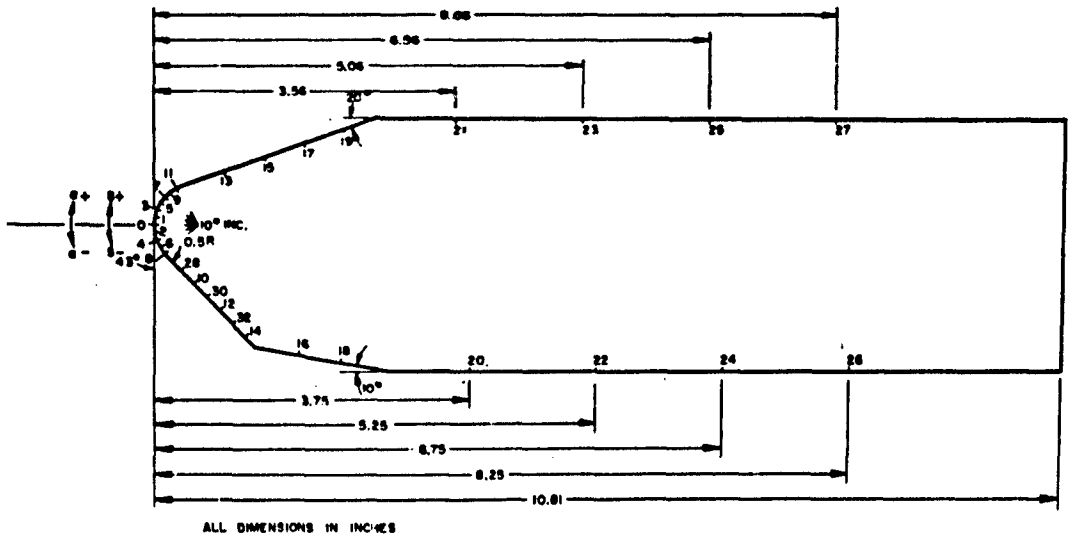

e. Modified Leading-Edge Model

Fig. 11 Concluded

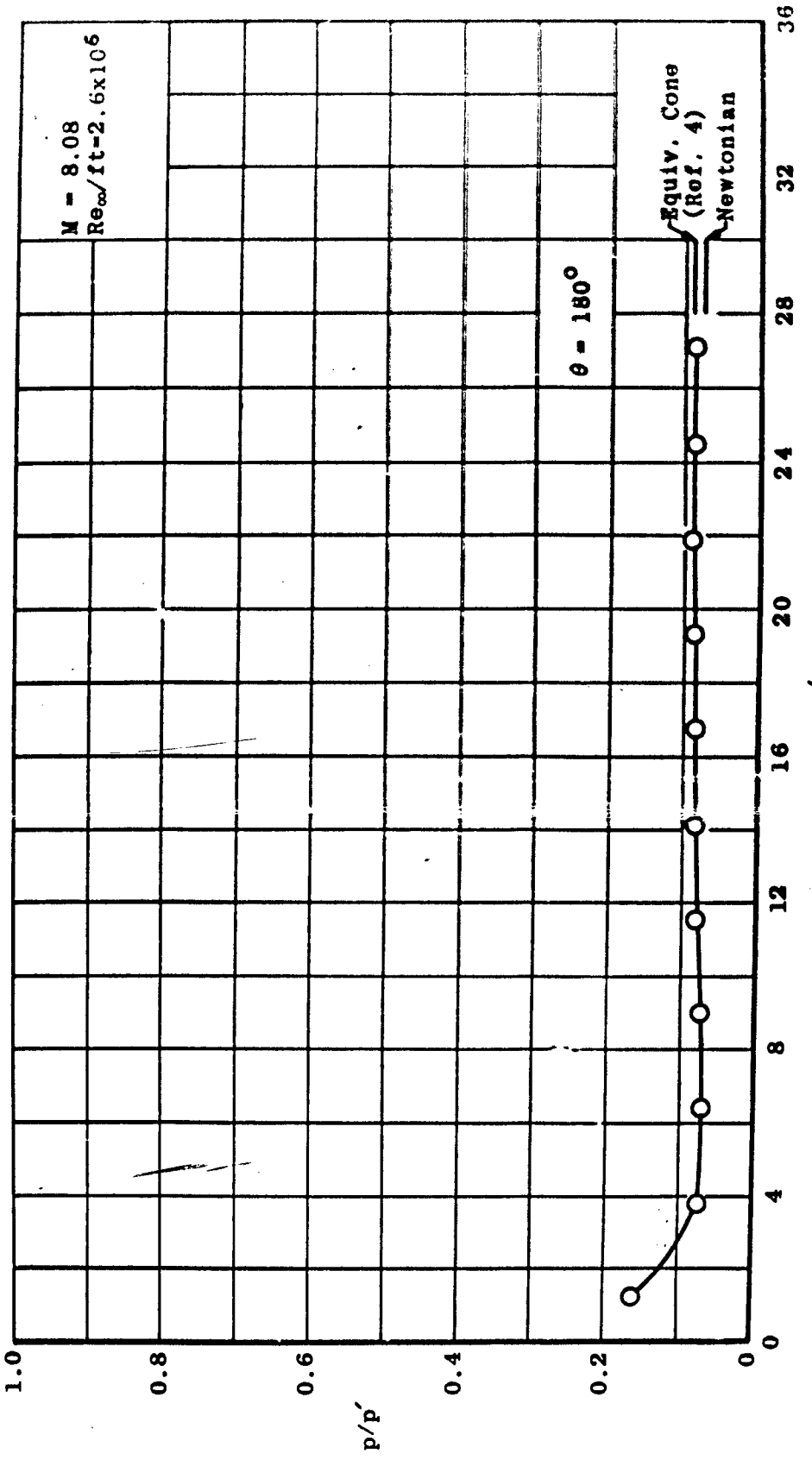

a. $\alpha = 0°$

Fig. 12 Axial Pressure Distribution on Cone Model

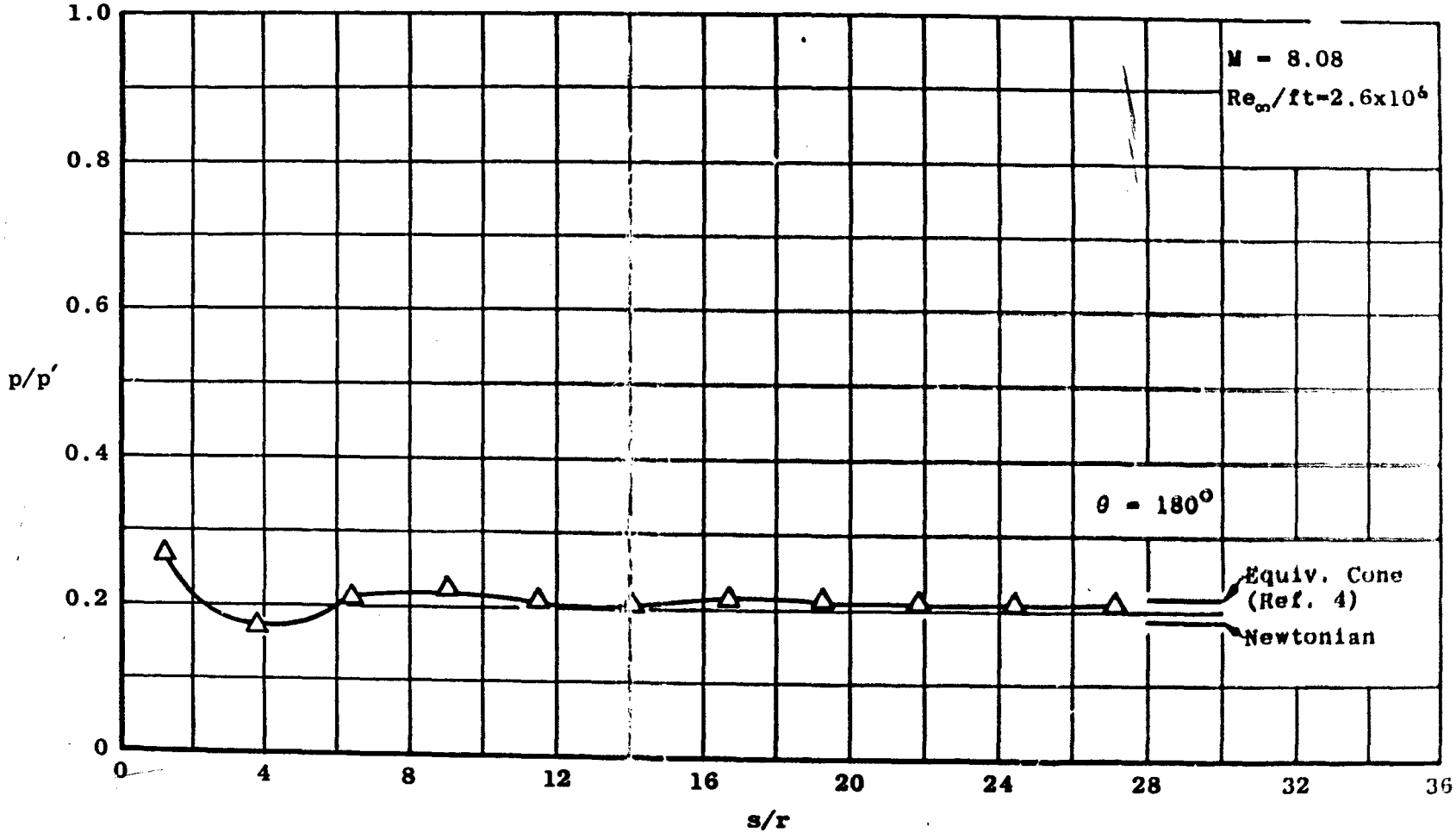

b. $\alpha = 10°$

Fig. 12 Continued

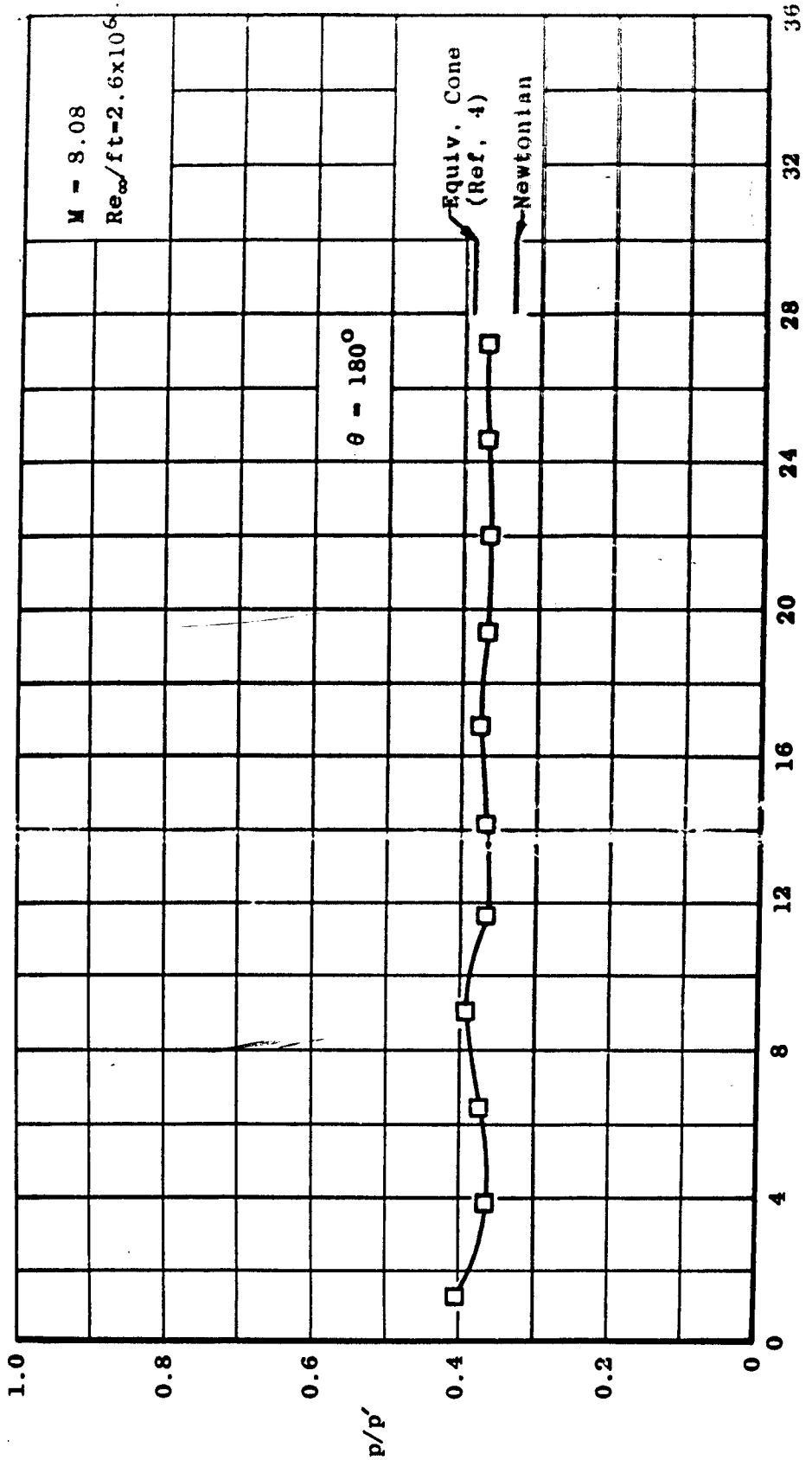

c. $\alpha = 20°$

Fig. 12 Continued

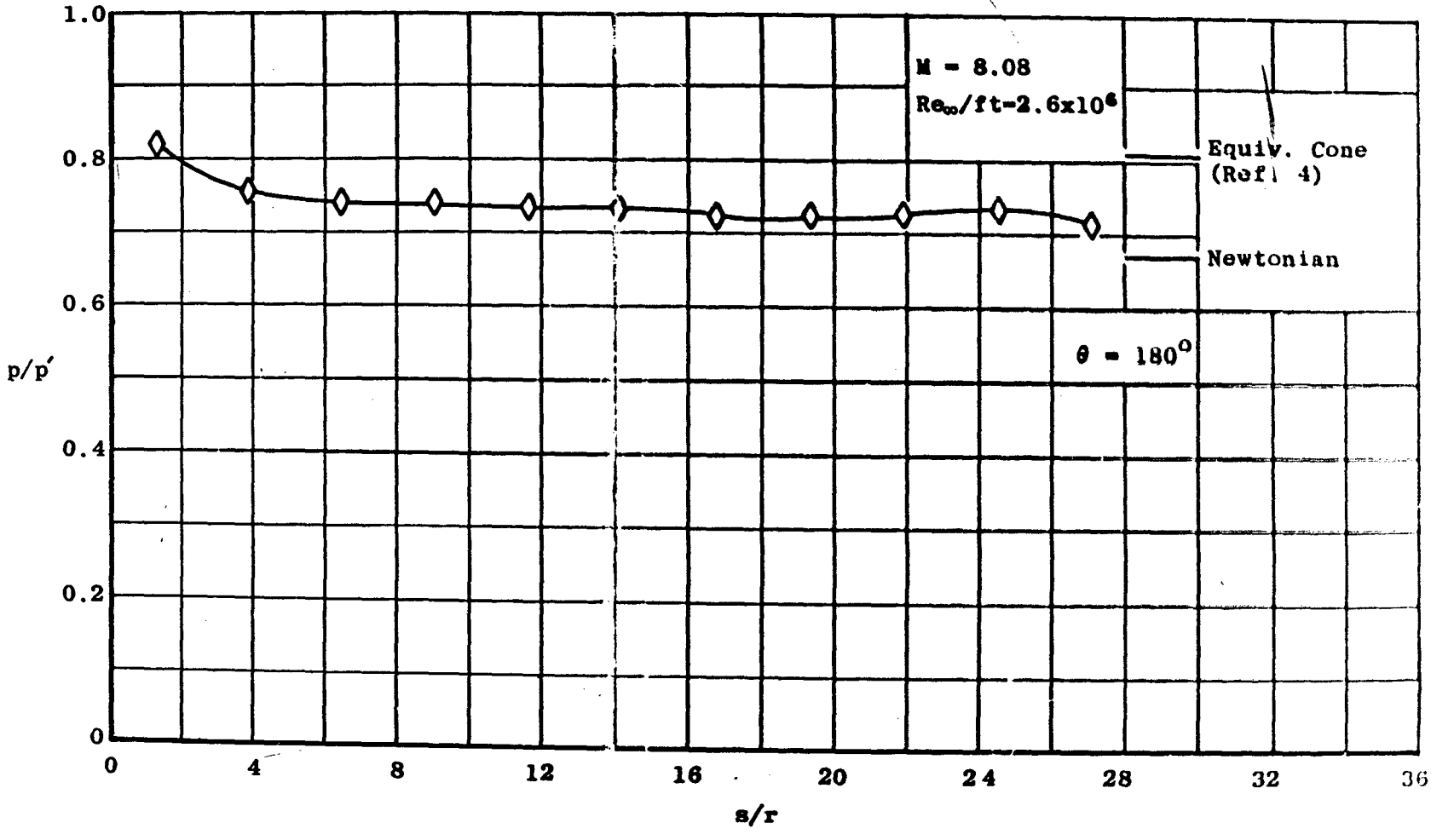

d. $\alpha = 40°$

Fig. 12 Continued

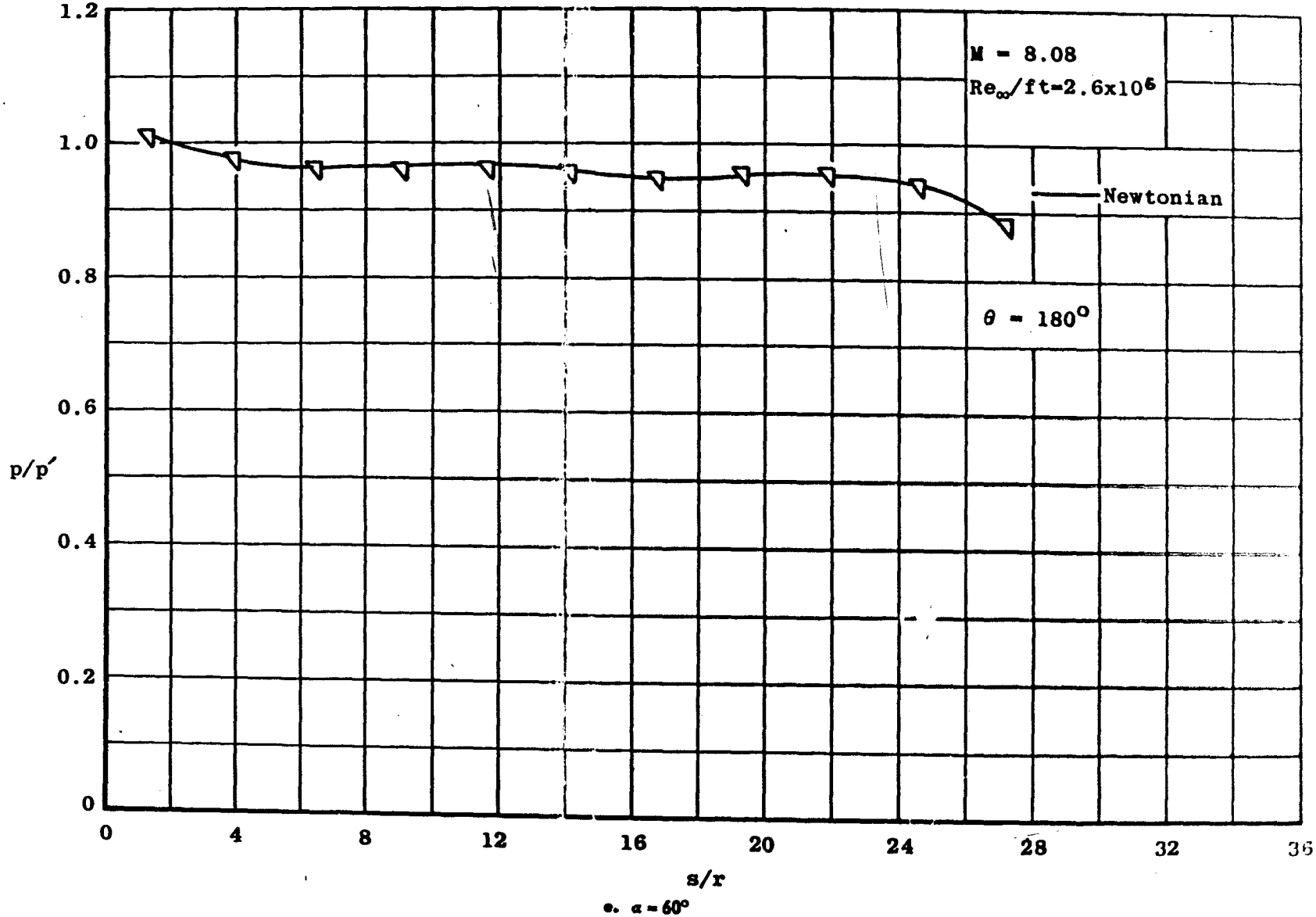

e. $\alpha = 60°$

Fig. 12 Concluded

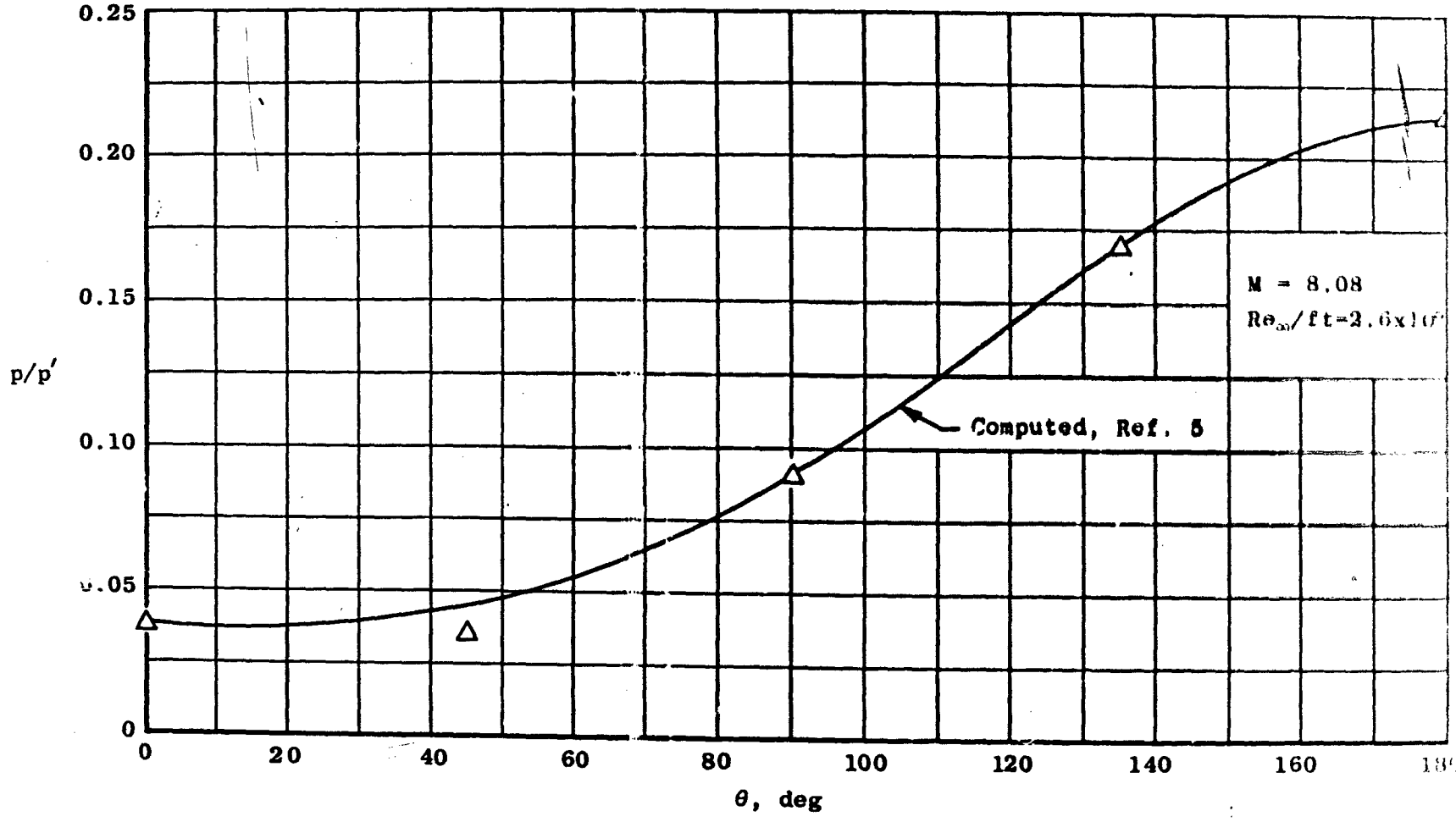

a. $\alpha = 10°$

Fig. 13 Peripheral Pressure Distribution on Cone Model

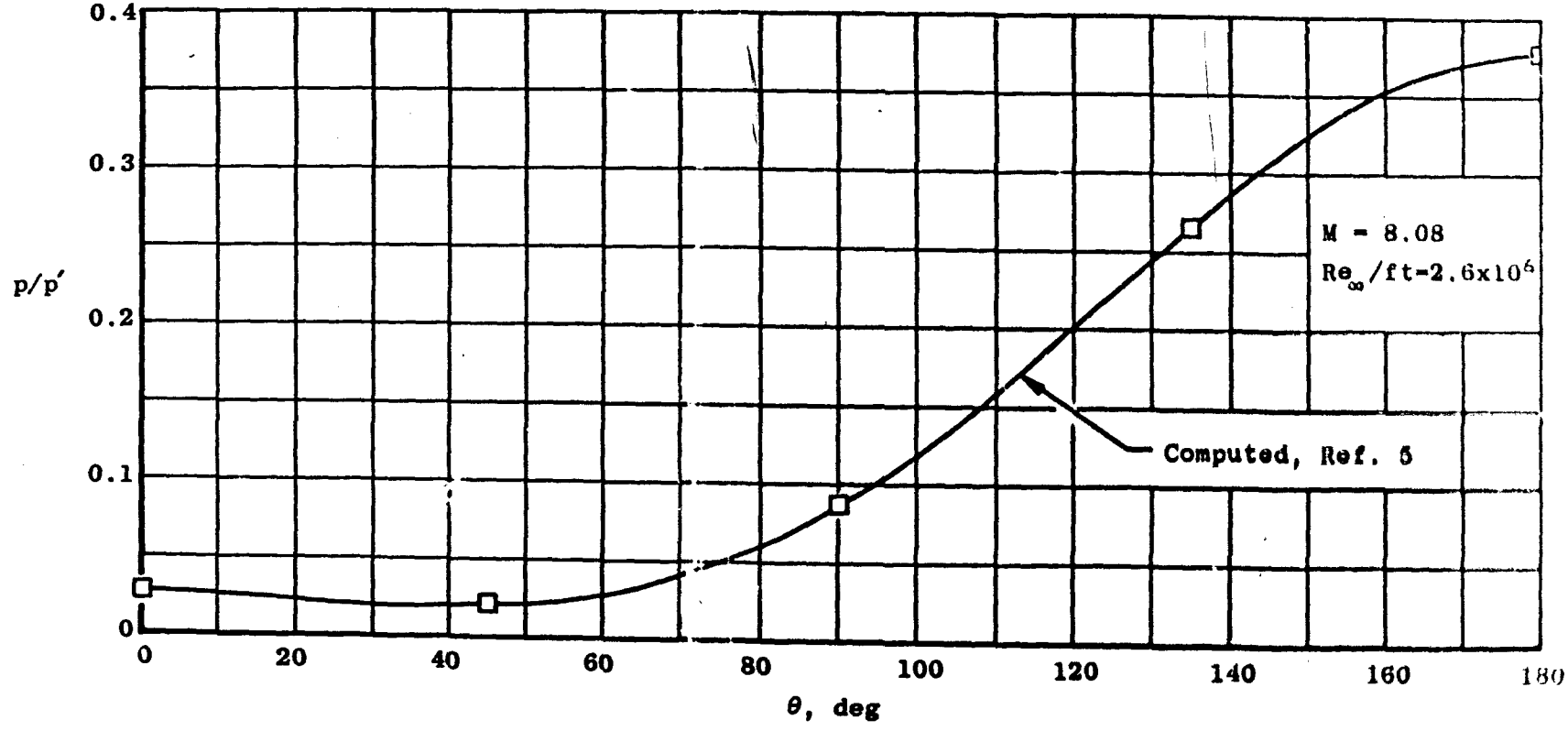

b. $\alpha = 20°$

Fig. 13 Continued

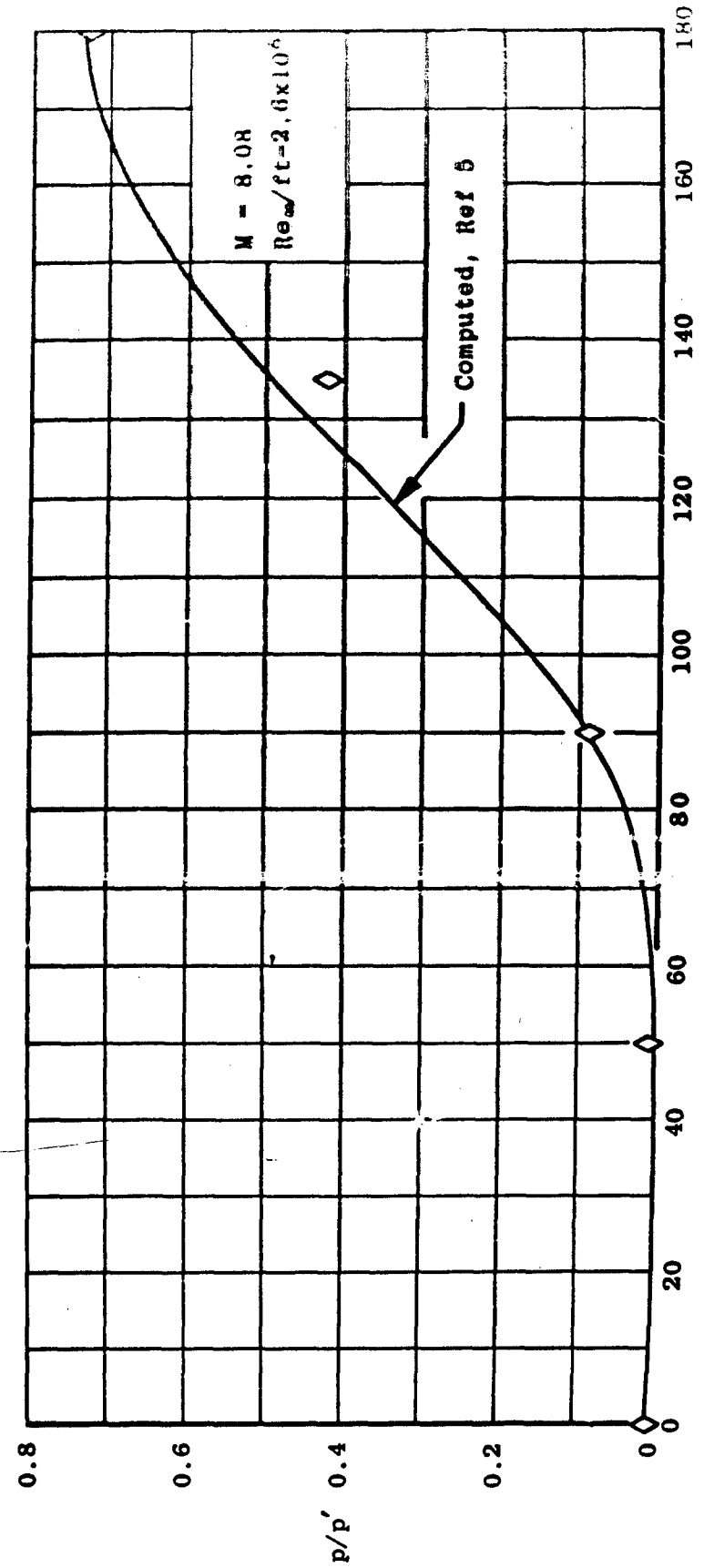

c. α = 40°

Fig. 13 Continued

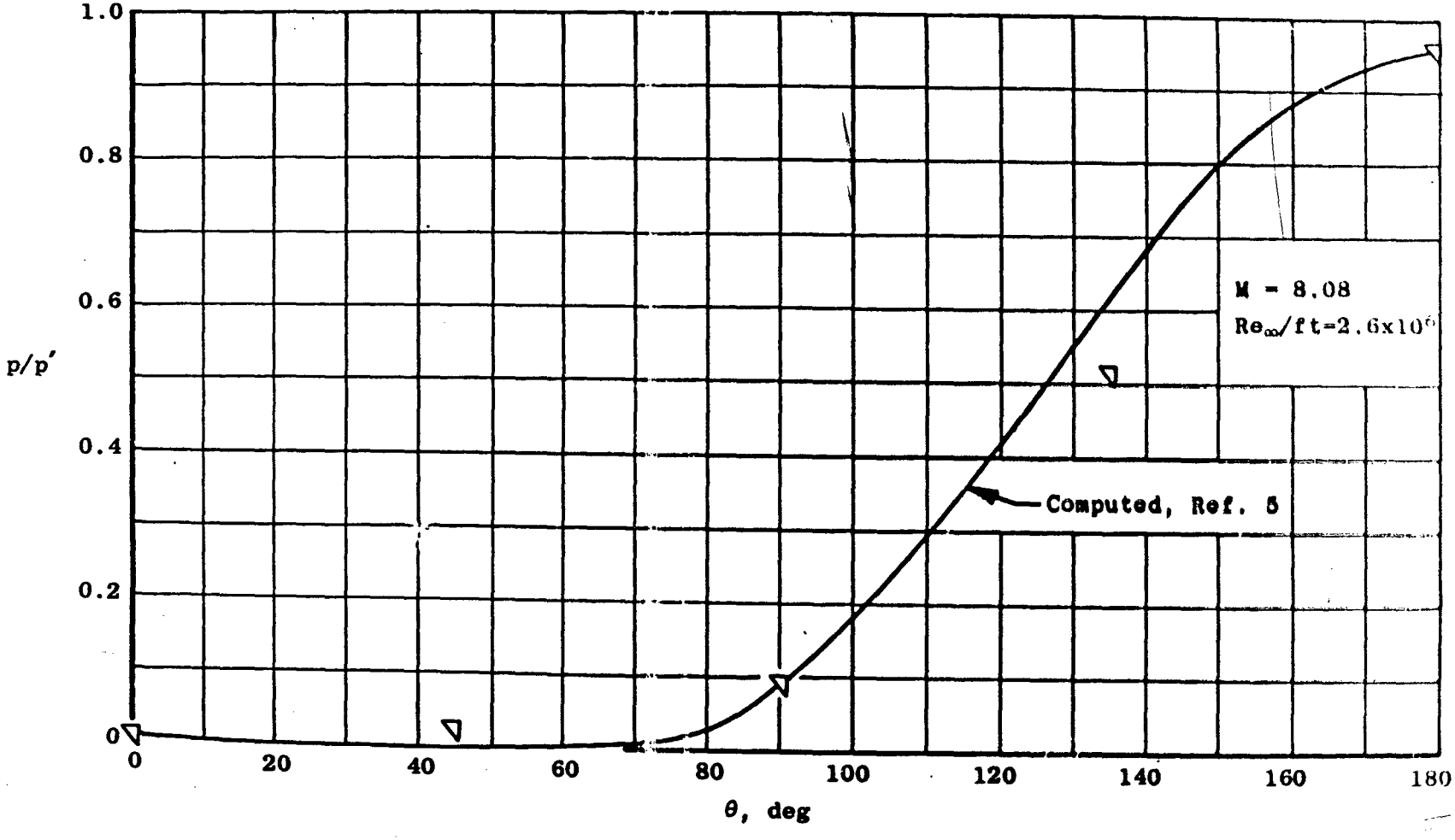

d. $\alpha = 60°$

Fig. 13 Concluded

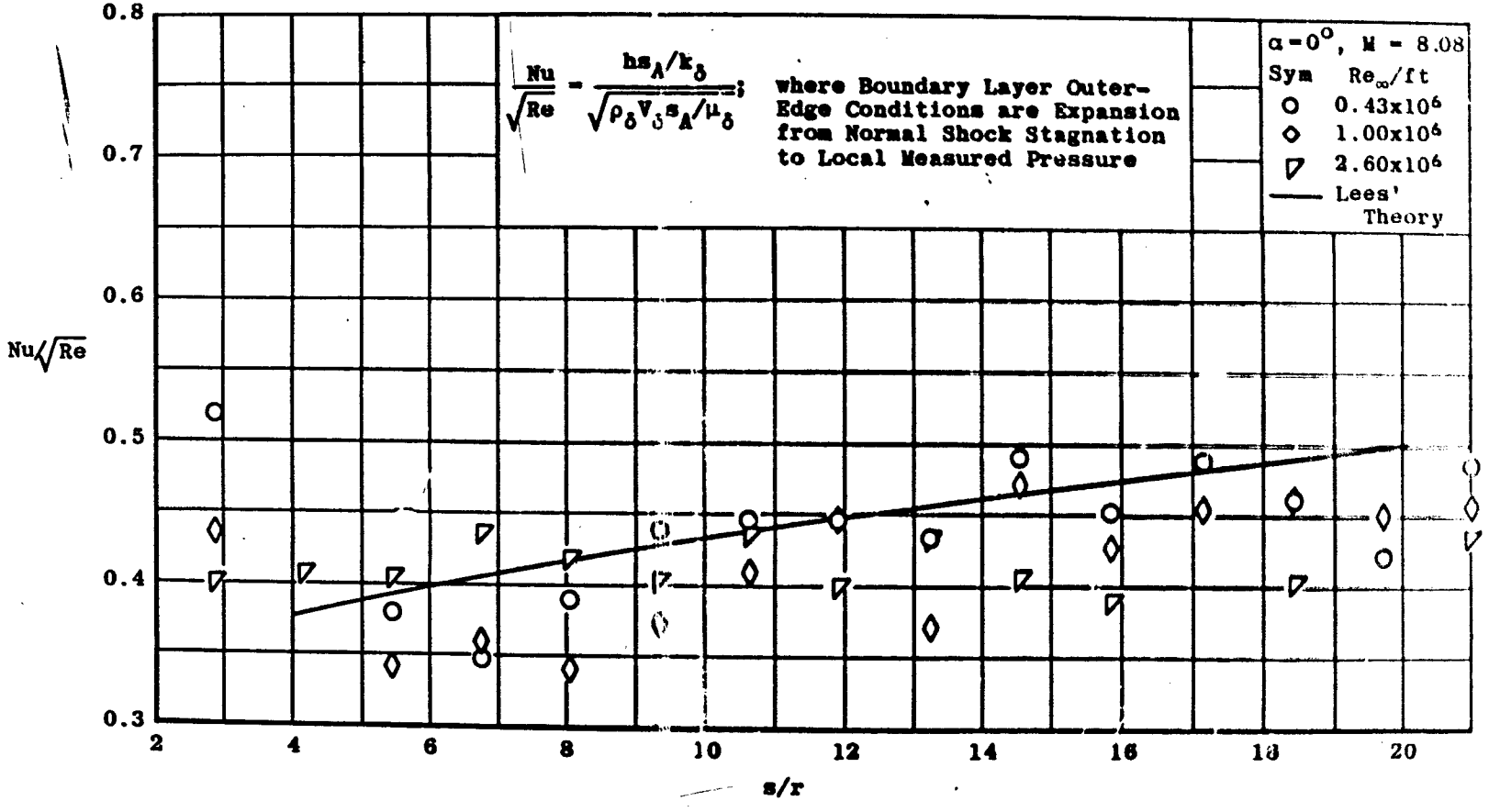

Fig. 14 Variation of Heat Transfer Parameter on Blunted Cone Model

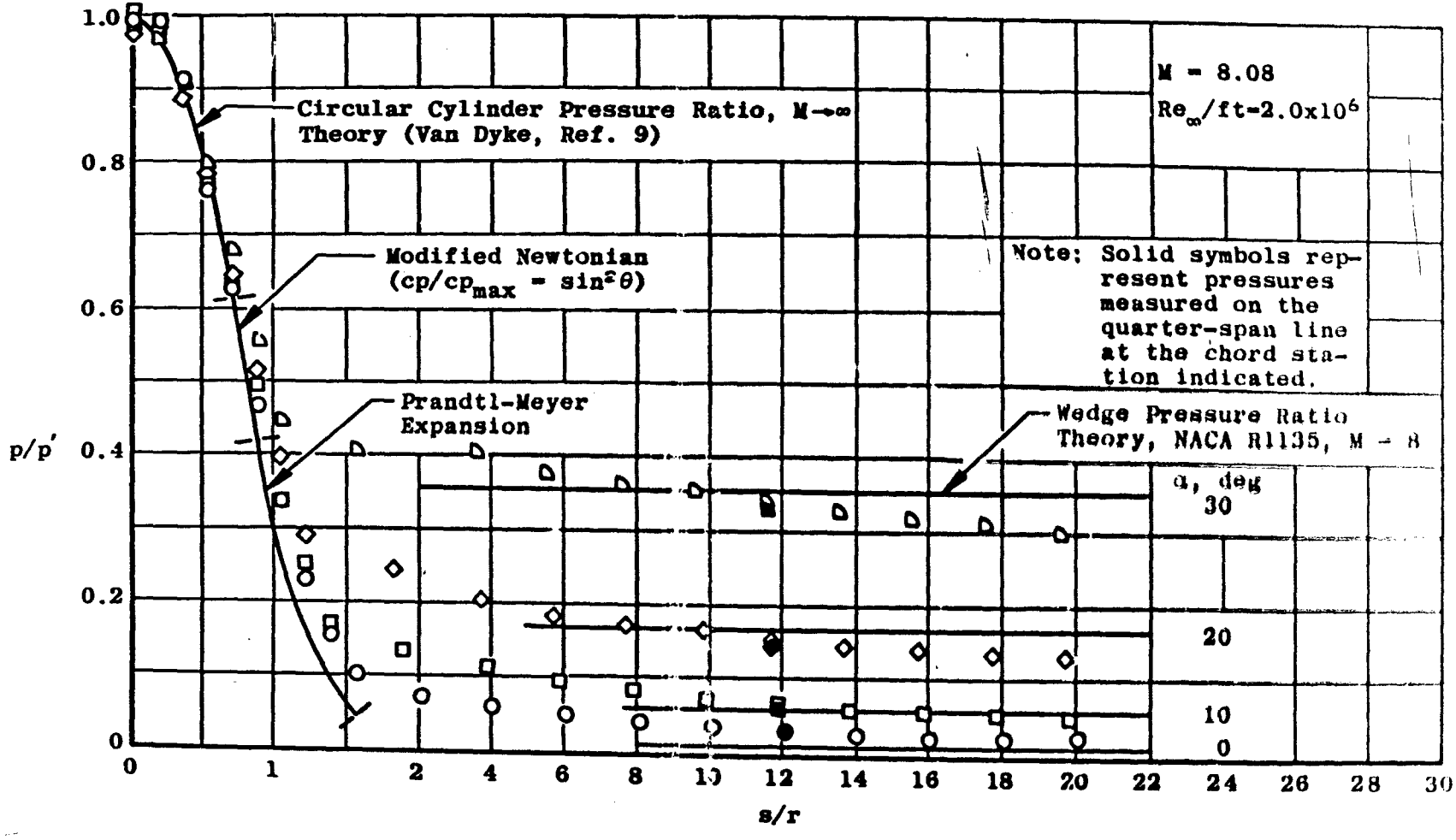

a. 0.05-in. Nose Radius

Fig. 15 Pressure Distribution on Cylindrically Blunt Flat Plate Models

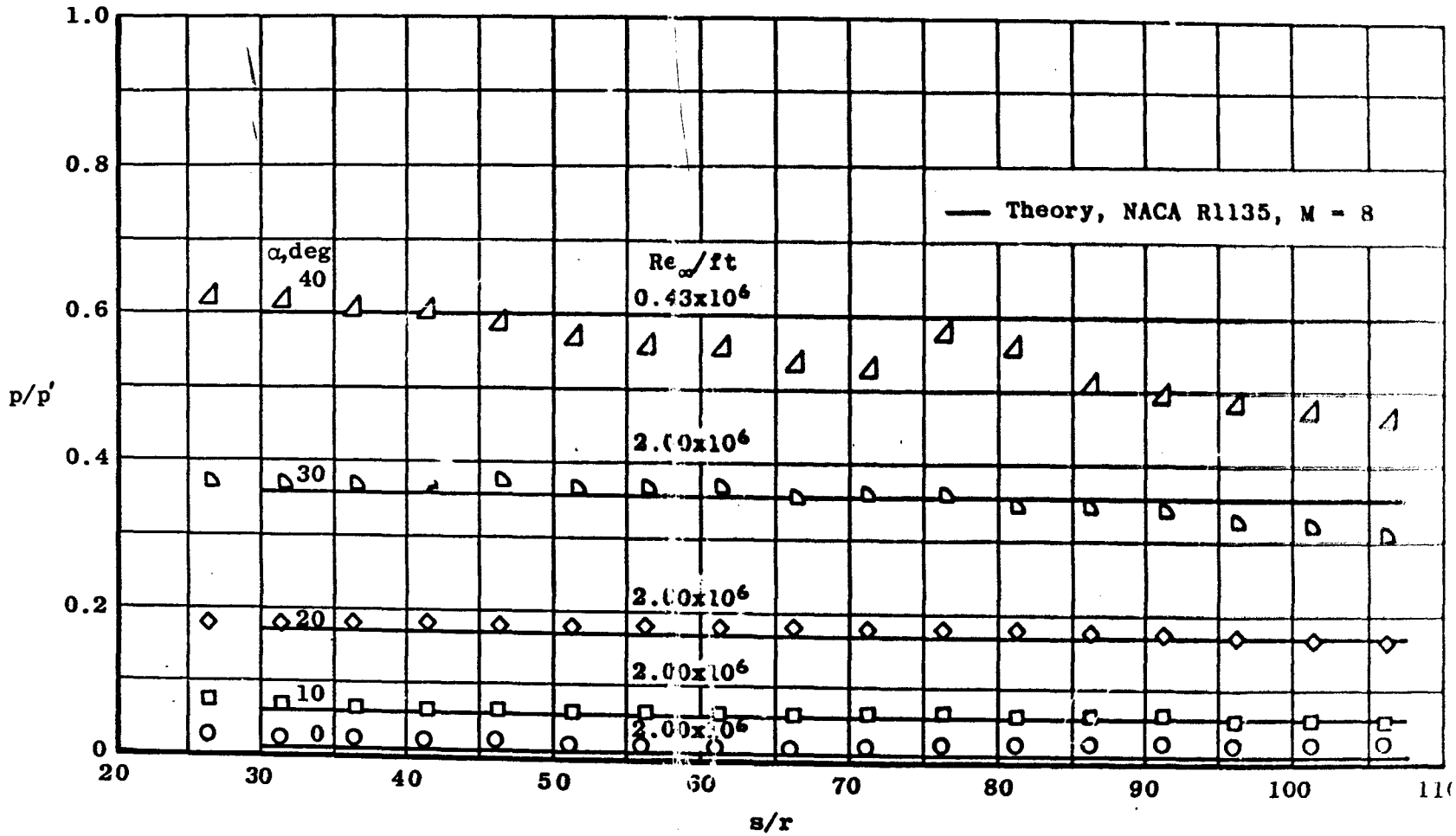

b. 0.10-in. Nose Radius

Fig. 35 Concluded

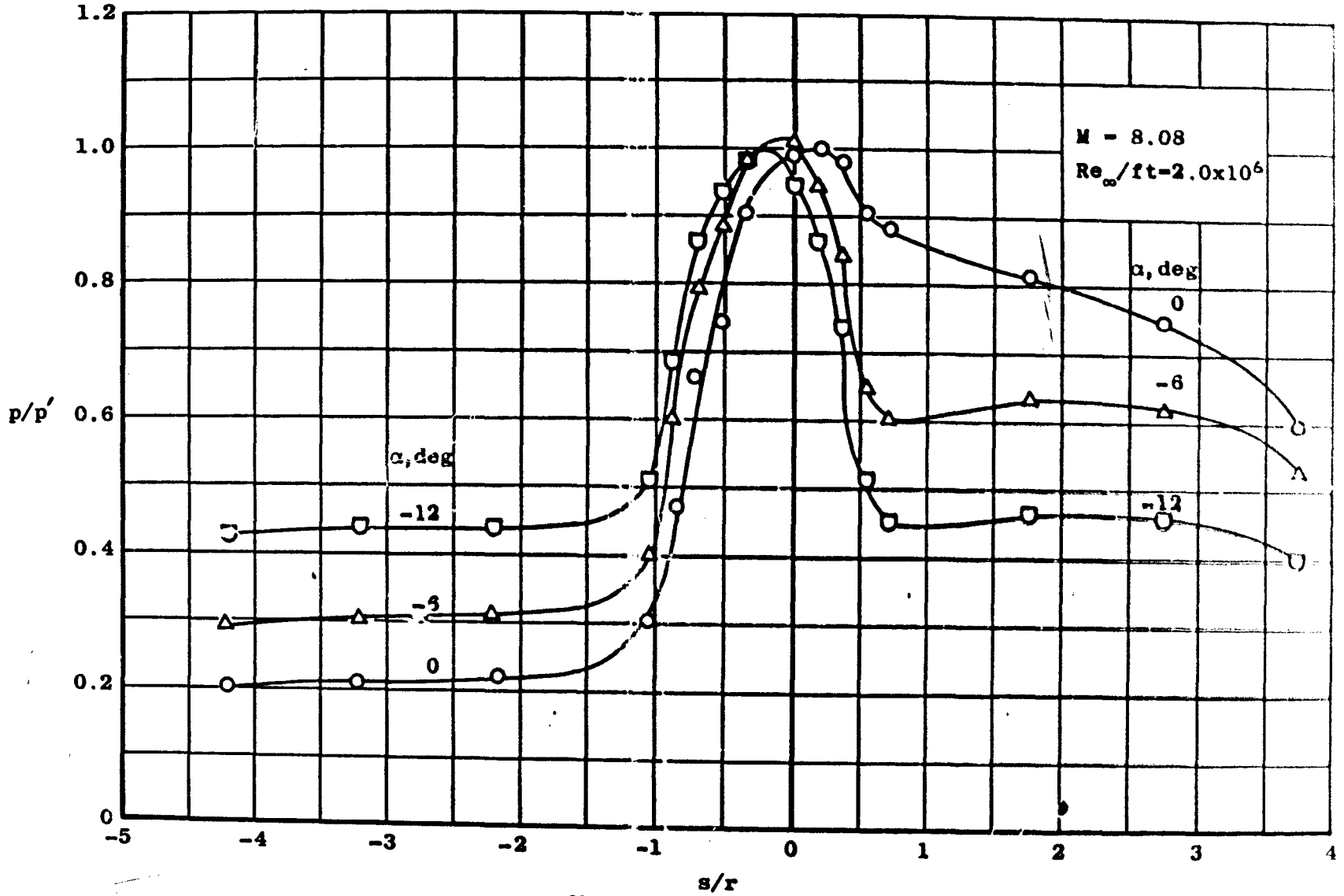

a. -12 to 0 deg Angle of Attack

Fig. 16 Pressure Distribution in Stagnation Region, Modified Leading-Edge Model

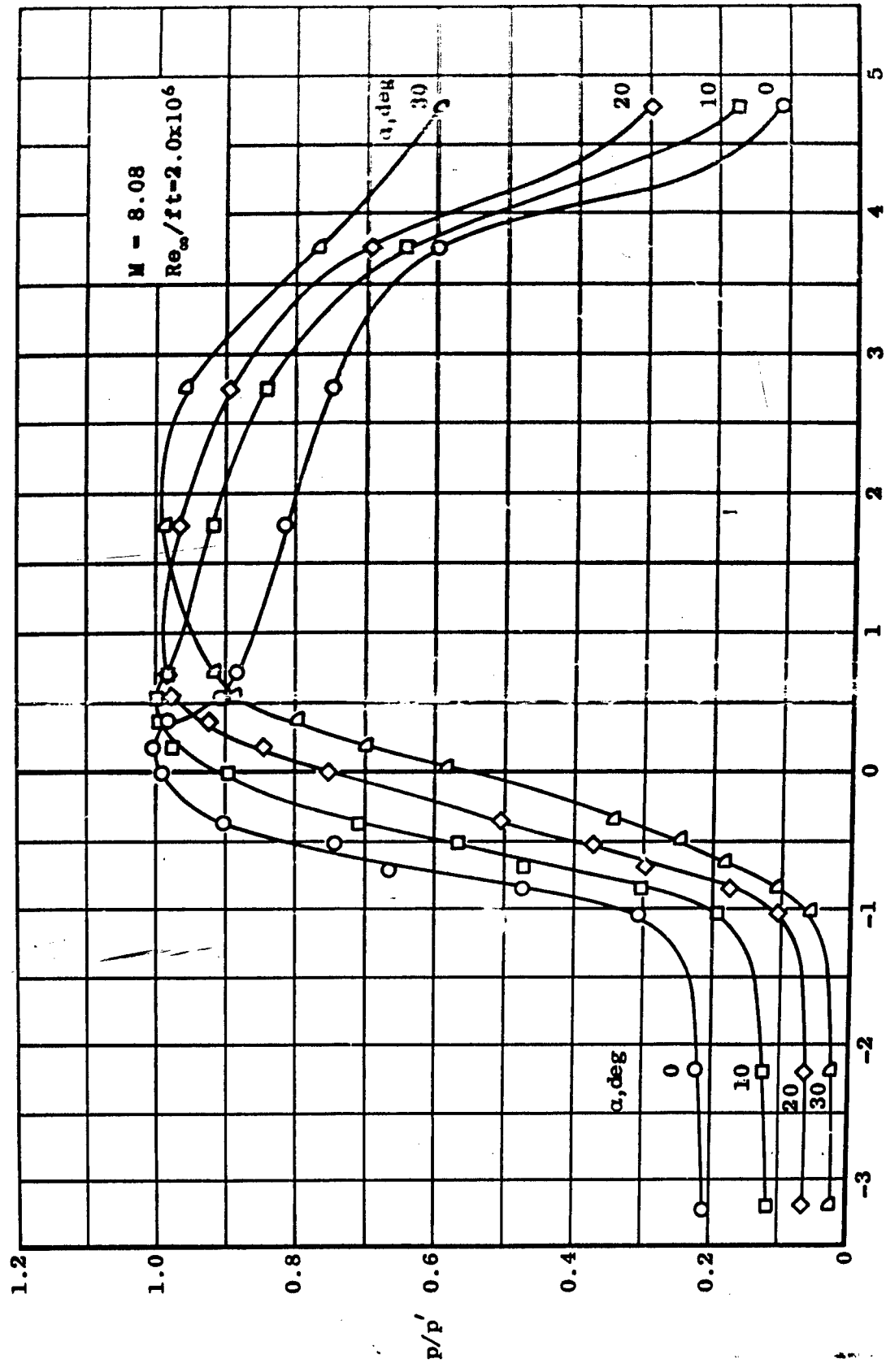

b. 0 to 30 deg Angle of Attack

Fig. 16 Concluded

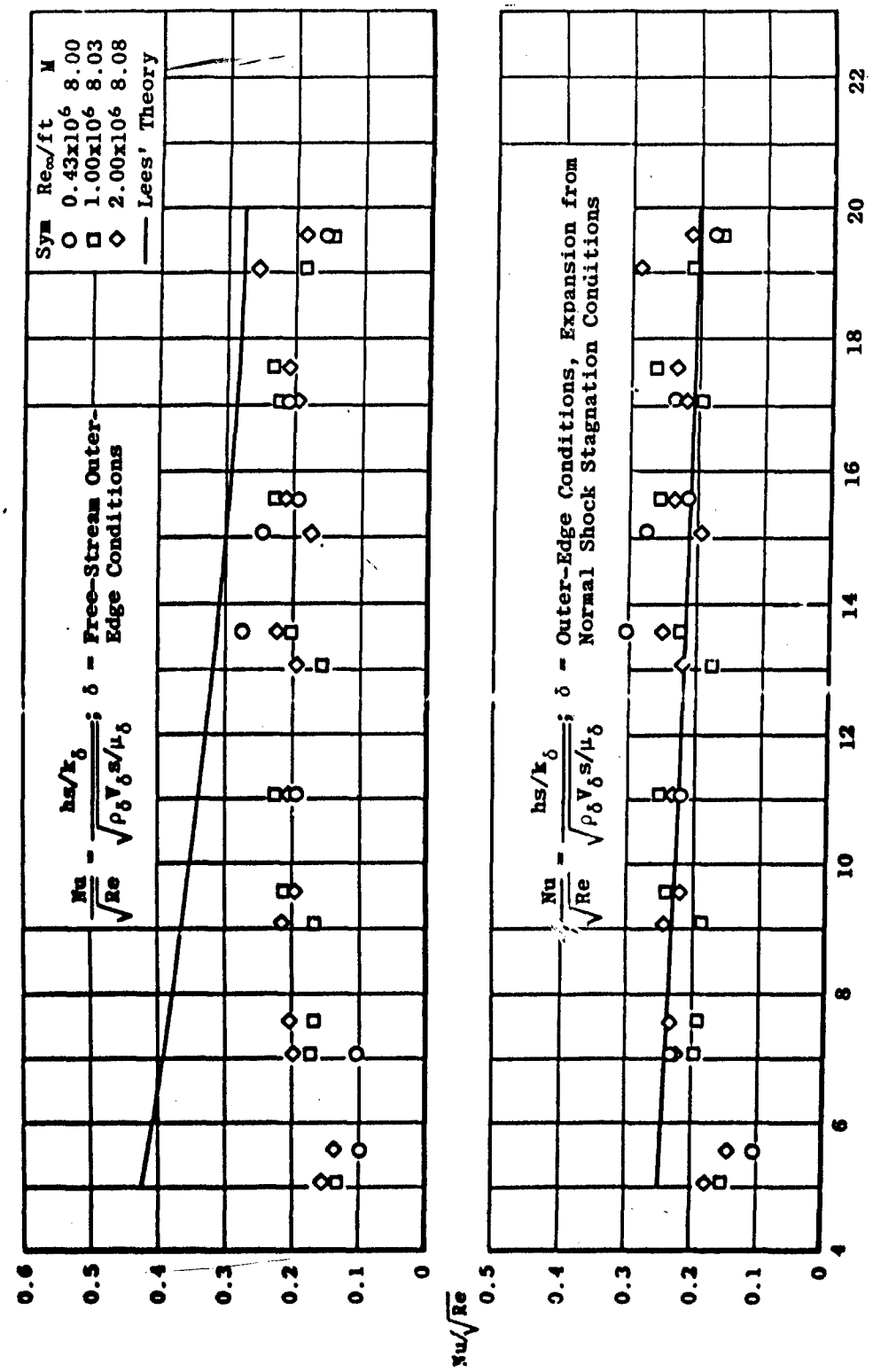

a. 0.50-in. Nose Radius Model

Fig. 17 Variation of Heat Transfer Parameter on Flat Plate Models

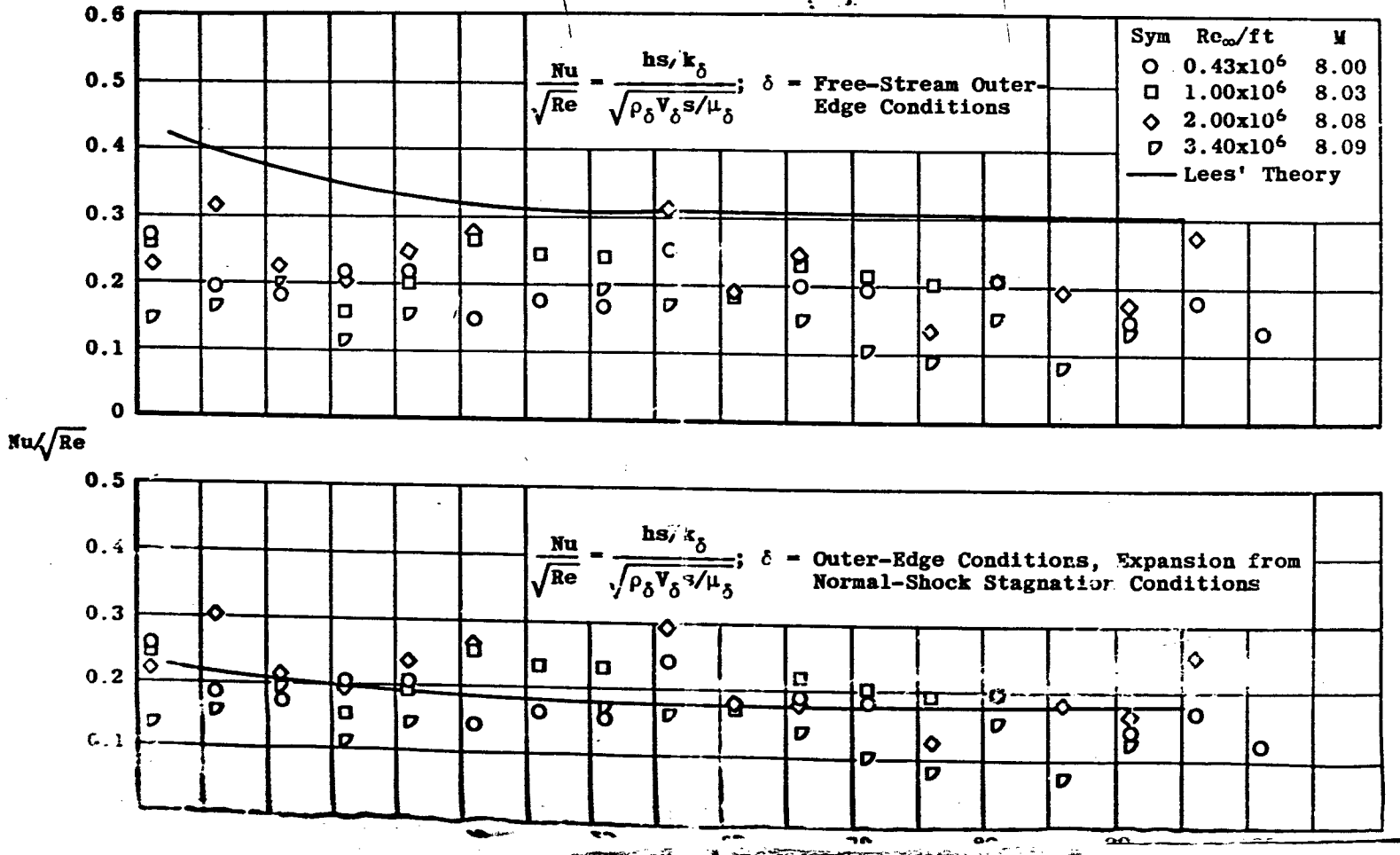
$\frac{Nu}{\sqrt{Re}} = \frac{hs/k_\delta}{\sqrt{\rho_\delta V_\delta s/\mu_\delta}}$; δ = Free-Stream Outer-Edge Conditions
Sym Re∞/ft M
0.43x10⁶ 8.00
1.00x10⁶ 8.03
2.00x10⁶ 8.08
3.40x10⁶ 8.09
Lees' Theory
$\frac{Nu}{\sqrt{Re}} = \frac{hs/k_\delta}{\sqrt{\rho_\delta V_\delta s/\mu_\delta}}$; δ = Outer-Edge Conditions, Expansion from Normal-Shock Stagnation Conditions
$Nu/\sqrt{Re}$
0.6
0.5
0.4
0.3
0.2
0.1
0
0.5
0.4
0.3
0.2
0.1